PART II

Observer Examples

Chapter 4

Linear Estimators and Observers for the Induction Machine (IM)

4.1. Introduction

Controlling alternating-current machines requires the implementation of complex algorithms for signal processing: the observation and estimation of quantities necessary for the control and regulation of output variables for speed drives made up of machines and associated static converters. To carry out these controls, it is necessary to have certain information for electrical and mechanical quantities measured from the power system. Ordinarily, these measures are obtained from physical sensors where the characteristics in terms of precision and bandwidth must be efficient, resulting in high cost for these devices and their maintenance, in addition to the significant structural fragility and sensitivity to unavoidable electromagnetic interferences. All these lead to a progressive suppression of physical sensors in relation to the mechanical structure of the machine, that is, flux, torque, rotation speed, and position sensors.

However, since knowing these quantities is vital for ensuring efficient control, estimators and observers constituting of indirect sensors were developed. The rest of this chapter explains several types of estimators and deterministic and stochastic observers. Order reduction methods are studied (see Chapter 5) to reduce calculation times. In this chapter, we will only consider linear structures of complete order observers, that is, on the basis of the hypothesis that mechanical modes (rotation speed and position) are infinitely slow compared to electrical modes, which enable

---

Chapter written by Maria PIETRZAK-DAVID, Bernard DE FORNEL and Alain BOUSCAYROL.

Electrical Actuators: Identification and Observation Edited by Bernard de Fornel and Jean-Paul Louis

us to consider rotation speed and position as parameters and thus ensure linearization of electrical equations.

The first section of this chapter mainly covers the estimation of magnetic stator and rotor or air-gap fluxes of the induction machine. In fact, the implementation of flux sensors in the air-gap is reserved for certain machines specifically used for benchmarks in university or industrial laboratories.

In the second part, we consider estimation and observation structures for defining the flux, torque, and rotation speed, while retaining linear or pseudolinear structures.

4.2. Estimation models for the induction machine

The goal of this preliminary section is to define models of the induction machine used to define magnetic flux estimators and observers. The hypotheses and validity ranges of the different structures studied will be deduced from the models presented.

4.2.1. *Park model for the induction machine*

4.2.1.1. *A dynamic model for observation*

Control and estimation of the induction machine require a dynamic model that is precise and simple enough to consider real-time implementation. The Park transformation satisfies this objective by using a magnetically equivalent orthonormal two-phase model. The speed of resolution, linked to the complexity of the model, is important for the use of observers and makes real-time implementation easier while ensuring estimation robustness.

The hypotheses required by the original three-phase model [CAR 95, PIE 88] are a sinusoidal distribution of the flux in the air-gap, no slot effect, no magnetic saturation, no account for thermal variations, particularly of the pellicular effect and hysteresis [CHA 83].

The Park transformation executes a change of reference frame between the initial three-phase variables and those of the magnetically equivalent two-phase model. A single orthonormal reference frame, judiciously chosen for all the (stator and rotor) variables, leads to certain simplifications of the model.

4.2.1.2. *Reference frame changes*

Different three-phase reference frames exist: the stator reference frame (1_S, 2_S, 3_S) linked to stator windings and rotor reference frame (1_R, 2_R, 3_R) linked to those

of the rotor (true windings for the wound machine or equivalent for the squirrel-cage machine). The reference frame (1_R, 2_R, 3_R) turns at rotation speed $\omega_{r/s}$[1] in relation to the stator (often called electric speed ω), directly linked to the mechanical speed of shaft Ω by the number of pole pairs P_p. The angular position of the rotor reference compared to that of stator $\theta_{r/s}$ (electrical position) is linked to the mechanical angular position of rotor θ:

$$\omega_{r/s} = \omega = P_p \cdot \Omega = \frac{d}{dt}\theta_{r/s} = P_p \cdot \frac{d}{dt}\theta \qquad [4.1]$$

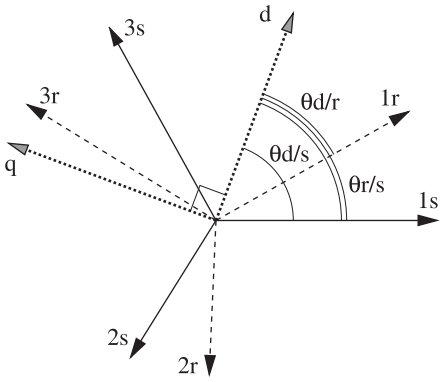

Figure 4.1. *Different study references frames*

We define a turning orthonormal reference frame (d,q) common to all variables used. It has an angular position $\theta_{d/s}$[2] (angular frequency, $\omega_{d/s}$) compared to reference frame (1_S, 2_S, 3_S), and angular position $\theta_{d/r}$[3] (angular frequency, $\omega_{d/r}$) compared to (1_R, 2_R, 3_R). The different positions (angular frequencies) are then linked by the main angular or frequency laws of the induction machine:

$$\theta_{d/s} = \theta_{d/r} + \theta_{r/s} \quad \text{or} \quad \omega_{d/s} = \omega_{d/r} + P_p \cdot \Omega \qquad [4.2]$$

Angular frequency $\omega_{d/s}$ corresponds to ω_s (power voltage angular frequency) in only sinusoidal mode, which explains the different indices.

The Park transformation changes the original three-phase reference frame to an orthonormal two-phase reference frame shifted by angle ρ [CHA 83]. If we do not

1 Index r/s for angular frequency (phase difference) of rotor (r) in relation to stator (s).

2 Index d/s for angular frequency (phase difference) of axis d compared to stator (s).

3 Index d/r for angular frequency (phase difference) of axis d compared to rotor (r).

take into consideration the homopolar component, the transformation is characterized by:

$$\left[P(\rho)\right] = \sqrt{\frac{2}{3}} \begin{bmatrix} \cos\rho & \cos\left(\rho - \frac{2\pi}{3}\right) & \cos\left(\rho + \frac{2\pi}{3}\right) \\ -\sin\rho & -\sin\left(\rho - \frac{2\pi}{3}\right) & -\sin\left(\rho + \frac{2\pi}{3}\right) \end{bmatrix} \quad [4.3]$$

Two Park transformations define an equivalent model in a single reference frame (d, q):

$$\underline{x}_{\mathrm{dq}} = \left[P(\theta_{\mathrm{d/s}})\right]\underline{x}_{\mathrm{ls2s3s}} \qquad \underline{x}_{\mathrm{dq}} = \left[P(\theta_{\mathrm{d/r}})\right]\underline{x}_{\mathrm{lr2r3r}} \quad [4.4]$$

We also use fixed reference frame (α_S, β_S) according to stator ($\theta_{\mathrm{d/s}} = 0$) and reference frame ($\alpha_R$, β_R) linked to rotor ($\theta_{\mathrm{d/r}} = 0$).

4.2.1.3. *The model in the general reference*

The dynamic model in any rotating reference frame (d, q), characterized by velocity $\omega_{\mathrm{d/s}}$ in relation to the stator and $\omega_{\mathrm{d/r}}$ in relation to the rotor is:

$$\begin{cases} V_{\mathrm{sd}} = R_{\mathrm{s}} I_{\mathrm{sd}} + \dfrac{\mathrm{d}}{\mathrm{d}t}\Phi_{\mathrm{sd}} - \omega_{\mathrm{d/s}}\Phi_{\mathrm{sq}} \\ V_{\mathrm{sq}} = R_{\mathrm{s}} I_{\mathrm{sq}} + \dfrac{\mathrm{d}}{\mathrm{d}t}\Phi_{\mathrm{sq}} + \omega_{\mathrm{d/s}}\Phi_{\mathrm{sd}} \\ V_{\mathrm{rd}} = R_{\mathrm{r}} I_{\mathrm{rd}} + \dfrac{\mathrm{d}}{\mathrm{d}t}\Phi_{\mathrm{rd}} - \omega_{\mathrm{d/r}}\Phi_{\mathrm{rq}} \\ V_{\mathrm{rq}} = R_{\mathrm{r}} I_{\mathrm{rq}} + \dfrac{\mathrm{d}}{\mathrm{d}t}\Phi_{\mathrm{rq}} + \omega_{\mathrm{d/r}}\Phi_{\mathrm{rd}} \end{cases} \quad [4.5]$$

Insofar as the machine is magnetically linear, the flux/current relations are linear with stator L_s and rotor L_r cyclic inductances, the mutual cyclic inductance between stator and rotor M_{sr} is given by:

$$\begin{cases} \Phi_{\mathrm{sd}} = L_{\mathrm{s}} I_{\mathrm{sd}} + M_{\mathrm{sr}} I_{\mathrm{rd}} \\ \Phi_{\mathrm{sq}} = L_{\mathrm{s}} I_{\mathrm{sq}} + M_{\mathrm{sr}} I_{\mathrm{rq}} \\ \Phi_{\mathrm{rd}} = M_{\mathrm{sr}} I_{\mathrm{sd}} + L_{\mathrm{r}} I_{\mathrm{rd}} \\ \Phi_{\mathrm{rq}} = M_{\mathrm{sr}} I_{\mathrm{sq}} + L_{\mathrm{r}} I_{\mathrm{rq}} \end{cases} \quad [4.6]$$

On the other hand, the electromagnetic torque is the result of the interaction between two fluxes and/or currents [CAR 95, PIE 88], for example:

$$T_{\text{em}} = P_{\text{p}} \frac{M_{\text{sr}}}{L_{\text{r}}} \left(\Phi_{\text{rd}} I_{\text{sq}} - \Phi_{\text{rq}} I_{\text{sd}} \right) \qquad [4.7]$$

The mechanical equation of the machine can be written as follows:

$$J \frac{\text{d}\omega_{\text{e}}}{\text{d}t} + f \omega_{\text{e}} = P_{\text{p}} (T_{\text{em}} - T_{\text{L}}) \qquad [4.8]$$

The general model, in any reference frame (d, q), is non-linear at order five, with four electrical variables (combination of currents and fluxes) and a mechanical variable, the machine's rotation speed. If we consider that the mechanical model is decoupled from magnetic and electrical modes (which is often the case), then the induction machine model is the association of two decoupled linear state systems: an order one system (mechanical part) and an almost stationary order four linear system (electrical part).

Most sinusoidal machines are squirrel-cage and their rotor voltage is zero.

4.2.2. *Different state models for flux estimation*

4.2.2.1. *State representation of a sinusoidal machine*

The previous hypothesis of mechanical and electromagnetic mode separation indicates that state variables [4.5] are components *d* and *q* of the stator and rotor fluxes. However, because of relations [4.6], different state vectors X can be chosen: stator and rotor currents, stator currents and stator fluxes. Obviously, the different associated state representations are equivalent and lead to identical dynamic behaviors [PIE 00, VUL 98]. For a squirrel-cage sinusoidal machine, control vector $\underline{\text{U}}$ is made up of stator voltages. Output vector $\underline{\text{Y}}$ is made up of stator currents that can be directly measured. Dynamic [A], control [B], and observation [C] matrices depend on the choice of $\underline{\text{X}}$:

$$\begin{cases} \dfrac{\text{d}}{\text{d}t} \underline{\text{X}} = [A] + [B] \underline{\text{U}} \\ \underline{\text{Y}} = [C] \underline{\text{X}} \end{cases} \qquad [4.9]$$

with:

$$\underline{U} = \underline{V}_{sdq} = \begin{bmatrix} V_{sd} & V_{sq} \end{bmatrix}^T \qquad \underline{Y} = \underline{I}_{sdq} = \begin{bmatrix} I_{sd} & I_{sq} \end{bmatrix}^T \qquad [4.10]$$

Among the different possibilities for the choice of state vector, we will retain three:

– the four fluxes;
– the stator fluxes and stator currents;
– the rotor fluxes and rotor currents;

4.2.2.2. *State vector made up of stator currents and fluxes*

The state vector is made up of axes d and q, components of the stator current and flux:

$$\underline{X} = \begin{bmatrix} i_{sd} & i_{sq} & \Phi_{sd} & \Phi_{sq} \end{bmatrix}^T \qquad [4.11]$$

The matrices of state equation come from this choice:

$$[A] = \begin{bmatrix} -(aR_S + bR_r) & \omega_{d/r} & aR_r / L_r & -a(\omega_{d/s} - \omega_{d/r}) \\ -\omega_{d/r} & -(aR_S + bR_r) & a(\omega_{d/s} - \omega_{d/r}) & aR_r / L_r \\ -R_S & 0 & 0 & \omega_{d/s} \\ 0 & -R_S & -\omega_{d/s} & 0 \end{bmatrix}$$

$$[B] = \begin{bmatrix} a & 0 \\ 0 & a \\ 1 & 0 \\ 0 & 1 \end{bmatrix} \quad \text{and} \quad [C] = \begin{bmatrix} 1 & 0 & 0 & 0 \\ 0 & 1 & 0 & 0 \end{bmatrix} \qquad [4.12]$$

$$a = \frac{1}{\sigma L_S} \quad b = \frac{1}{\sigma L_r} \quad c = \frac{1-\sigma}{\sigma M_{sr}} \quad \sigma = 1 - \frac{M_{sr}^2}{L_S L_r} \qquad [4.13]$$

This representation is used for controls based on the stator flux (DTC, stator flux vector control, etc.). In addition, it makes it possible to estimate the stator flux. The output vector corresponds to a state vector, relatively important property in terms of precision and robustness of the different observers studied, or to the implementation of a reduced order observer (Chapter 5).

4.2.2.3. *State vector made up of stator currents and rotor fluxes*

The state vector is:

$$\underline{X} = \begin{bmatrix} i_{sd} & i_{sq} & \Phi_{rd} & \Phi_{rq} \end{bmatrix}^T \quad [4.14]$$

New state matrices are:

$$[A] = \begin{bmatrix} -aR_s - (1-\sigma)bR_r & \omega_{d/s} & cR_r / L_r & c(\omega_{d/s} - \omega_{d/r}) \\ -\omega_{d/s} & -aR_s - (1-\sigma)bR_r & -c(\omega_{d/s} - \omega_{d/r}) & cR_r / L_r \\ R_r M_{sr} / L_r & 0 & -R_r / L_r & \omega_{d/r} \\ 0 & R_r M_{sr} / L_r & -\omega_{d/r} & -R_r / L_r \end{bmatrix}$$

$$[B] = \begin{bmatrix} a & 0 \\ 0 & a \\ 0 & 0 \\ 0 & 0 \end{bmatrix} \quad \text{and} \quad [C] = \begin{bmatrix} 1 & 0 & 0 & 0 \\ 0 & 1 & 0 & 0 \end{bmatrix} \quad [4.15]$$

This representation is used for controls based on the rotor flux (vector control) direction. This state model has the same properties as the previous model [4.11] and can therefore lead to a rotor flux reduced observer and good robustness of observers (output vector corresponding to a part of the state vector).

4.2.2.4. *State vector made up of stator fluxes and rotor fluxes*

The state vector is then:

$$\underline{X} = \begin{bmatrix} \Phi_{sd} & \Phi_{sq} & \Phi_{rd} & \Phi_{rq} \end{bmatrix}^T \quad [4.16]$$

$$[A] = \begin{bmatrix} -aR_s & \omega_{d/s} & cR_s & 0 \\ -\omega_{d/s} & -aR_s & 0 & cR_s \\ cR_r & 0 & -bR_r & \omega_{d/r} \\ 0 & cR_r & -\omega_{d/r} & -bR_r \end{bmatrix}$$

New state matrices are obtained:

$$[\mathrm{B}] = \begin{bmatrix} 1 & 0 \\ 0 & 1 \\ 0 & 0 \\ 0 & 0 \end{bmatrix} \quad \text{and} \quad [\mathrm{C}] = \begin{bmatrix} a & 0 & -c & 0 \\ 0 & a & 0 & -c \end{bmatrix} \qquad [4.17]$$

This representation can be used for the development of a control based on stator or rotor flux, or on both [JAN 94]. Even though this model may seem more universal than the previous ones, it cannot result in reduced order observers (no variables can be easily measured in the state vector). In addition, the convergence of the output vector does not condition that of the state vector: matrix [C] contains parameters sensitive to variations.

4.2.3. *Different study reference frames for flux estimation*

4.2.3.1. *Different study reference frames*

The ordinary orthonormal two-phase reference frame is not optimal, and additional simplifications are linked to specific choices. We can observe two categories of references based on the determination of angles.

The first one corresponds to transformation angles directly deducted from the measures of stator currents. We then speak of direct flux estimations.

In the second one, the angles are first determined from the estimation algorithm itself. The evolution of variables must be insignificant for the calculation period (quasi-stationarity). This hypothesis applies to matrix A in which the speed is considered as a parameter. We then speak of indirect estimations. In all discretized observers, the inputs are considered as constant during the sampling period. The flux vector can be estimated in Cartesian or polar form. In the first case, reference frame (d, q) is not necessarily aligned with the flux vector considered. From these Cartesian components, we can easily calculate its polar components:

$$|\underline{\Phi}| = \sqrt{\Phi_{\mathrm{d}}^2 + \Phi_{\mathrm{q}}^2} \qquad \theta_{\Phi} = \arg \Phi = \operatorname{actg}\left(\Phi_{\mathrm{q}} / \Phi_{\mathrm{d}}\right) \qquad [4.18]$$

When the reference is aligned with the flux vector to estimate its polar coordinates and components on another reference frame (d′, q′) out of phase by φ, are:

$$\Phi_{\mathrm{d}'} = \Phi_{\mathrm{d}} \cos\varphi \qquad \Phi_{\mathrm{q}'} = \Phi_{\mathrm{d}} \sin\varphi \qquad [4.19]$$

The dynamic behavior of the machine will be different according to the reference. This is caused by the non-linear Park transformation (depends on a variable angle). Reference (α_S, β_S) (*d* aligned with a stator phase) is the one that has the closest dynamic behavior to the real machine [BEN 93, OUR 95, VUL 98, WES 94], because it uses a linear transformation for stator variables (Concordia transformation).

4.2.3.2. *Reference frames based on prior knowledge of angles*

In reference frame (α_S, β_S) set in relation to the stator, the angular positions of the different references are $\theta_{d/s} = 0$ and $\theta_{d/r} = -P_p \cdot \Theta$.

The reference frame change of stator variables occurs according to the Concordia transformation. The reference change of rotor variables requires the measure of shaft position Θ (position sensor) or the integrated rotation speed of shaft Ω (velocity rotation speed sensor). The global model [4.5] and estimation structures are simplified.

Stationary reference frame (α_R, β_R) in relation to the rotor has dual properties. A position or velocity sensor makes it possible to deduce the angle of transformation. The model and estimations in this reference frame are simplified because:

$$\theta_{d/r} = 0 \quad \text{and} \quad \theta_{d/s} = P_p \cdot \Theta$$

A third reference frame (d,q), aligned with the stator current [ROB 92], can be used for a direct determination of the transformation angle. The measured stator currents and their components in reference frame (α_S, β_S) result in the polar coordinates of the current [4.17] and thus the transformation angles.

4.2.3.3. *Reference frames based on subsequent knowledge of angles*

The other references frame (d, q) use subsequent knowledge of transformation angles. The most widely used are references linked to the desired flux: d linked to stator flux ($\Phi_{sq} = 0$) or rotor flux ($\Phi_{rq} = 0$). In fact, these two references make it possible to simplify controls for stator or rotor flux controls. They can be used to directly determine the polar components of these fluxes. The flux estimation in one of these reference frames depends on the stator current components and the transformation angle linked to this reference. This angle is deducted from flux estimates. We can see that there is looping (Figure 4.3), representing the rotor flux estimator. The validity of the estimation therefore depends on the quasi-stationarity of model variables in relation to the calculation step and error, between the estimated and true angle, which is then ignored.

4.2.3.4. *Assessment of the different reference frames appropriate for the estimation of fluxes*

For a squirrel-cage induction machine, the reference that is best adapted to the estimation of fluxes is reference frame (α_S, β_S). Reference frame (d, q) linked to the stator current offers the possibility of a direct knowledge of angles of transformation by introducing a non-linearity linked to the transformation.

For simplicity reasons, we can use a reference frame (d, q) linked to the flux considered because it directly leads to the polar coordinates of this flux. On the other hand, during real-time implementation of the estimation algorithm, as long as we verify the quasi-stationarity of the variables in relation to the calculation time.

4.3. Flux estimation

4.3.1. *Introduction*

The magnetic flux of the induction machine is one of the fundamental quantities necessary for the correct control of torque and thus velocity, and possibly the mechanical position of the machine. It is possible to observe three types of estimation structures:

- open loop estimators [PIE 00];
- Luenberger deterministic observers [LUE 71];
- Kalman–Bucy stochastic observers [KAL 82].

The first category consists of combining circuits or algorithms on the basis of all or part of the machine model, with no correction and therefore functioning in open loop. These estimators are mainly characterized by their simplicity, so there are very few calculation means. The downside is their dependence on real system's time constants, resulting in a slow convergence. We also note a strong dependence on structural and functional speed drive parameters, leading to errors and even in certain cases, to instabilities.

The deterministic state observers have a more complex structure; hence the more significant calculation means. But they work in closed loop, and an error detected and amplified is used to correct the operation and enables the convergence based on a time constant depending on the amplification gain, with a theoretically zero error. They have an inherent dynamic independent from the system. The robustness in relation to parameters is better than in the previous case.

Stochastic observers have structures comparable to the previous ones, but with a consideration for state noises and measuring noises, leading to a smoothing of operations that guarantee better stabilization and robustness than the deterministic observer.

4.3.2. *Stator flux estimator*

We consider flux estimator [ARC 99] (Figure 4.2) used particularly in DTC control. From the measure of two stator voltages and two currents: i_{s1}, i_{s2} and V_{s1}, V_{s2}, we rebuild the components of the stator or rotor flux in fixed two-phase axes $\alpha\beta$:

$$i_{s\alpha} = \frac{\sqrt{3}}{2} i_{s1} \quad \text{and} \quad i_{s\beta} = \frac{1}{\sqrt{2}} \left(i_{s1} + 2 i_{s2} \right) \qquad [4.20a]$$

and similarly:

$$V_{s\alpha} = \frac{\sqrt{3}}{2} V_{s1} \quad \text{and} \quad V_{s\beta} = \frac{1}{\sqrt{2}} \left(V_{s1} + 2 V_{s2} \right) \qquad [4.20b]$$

In this reference frame, the stator equations are:

$$\begin{aligned} V_{s\alpha} &= R_s i_{s\alpha} + \frac{\mathrm{d}}{\mathrm{d}t} \Phi_{s\alpha} \\ V_{s\beta} &= R_s i_{s\beta} + \frac{\mathrm{d}}{\mathrm{d}t} \Phi_{s\beta} \end{aligned} \qquad [4.21]$$

Hence, the flux components in this fixed reference are:

$$\begin{aligned} \Phi_{s\alpha} &= \int \left(V_{s\alpha} - R_s i_{s\alpha} \right) \mathrm{d}t \\ \Phi_{s\beta} &= \int \left(V_{s\beta} - R_s i_{s\beta} \right) \mathrm{d}t \end{aligned} \qquad [4.22]$$

and the three-phase RMS value of stator flux Φ_s is:

$$\Phi_s = \frac{1}{\sqrt{3}} \sqrt{\Phi_{s\alpha}^2 + \Phi_{s\beta}^2} \qquad [4.23]$$

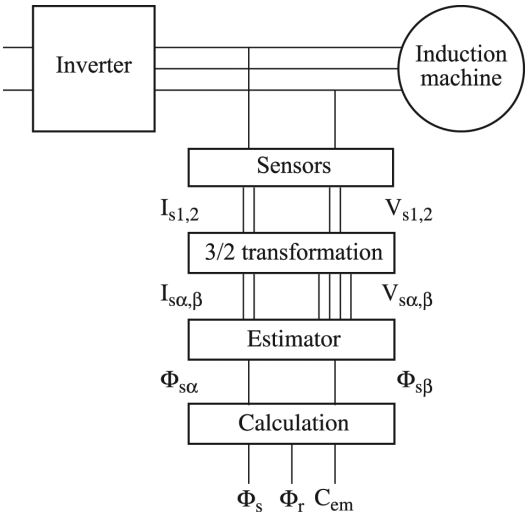

Figure 4.2. *Stator and rotor flux and electromagnetic torque estimator*

The rotor flux components are deducted from those of the stator fluxes and currents, according to relations:

$$\begin{aligned} \Phi_{r\alpha} &= \frac{L_r}{M_{sr}}\Phi_{s\alpha} - \sigma L_s i_{s\alpha} \\ \Phi_{r\beta} &= \frac{L_r}{M_{sr}}\Phi_{s\beta} - \sigma L_s i_{s\beta} \end{aligned} \qquad [4.24]$$

We notice that the stator flux depends on a single parameter: stator resistance. The estimation error will therefore be more significant at very low frequency, thus at very slow rotation speed. Knowing fluxes and currents, we deduce the electromagnetic torque:

$$T_{em} = P_p\left[\Phi_{s\alpha}\cdot i_{s\beta} - \Phi_{s\beta}\cdot i_{s\alpha}\right] \qquad [4.25]$$

One of the weak points of this estimator is the open loop integration of electromotive force, which results in errors. However, its great simplicity leads to its use, especially for direct scalar control and DTC. Instead of using two voltage sensors, we can reconstitute stator voltage from the converter control (as long as dead time can be compensated) and the *continuous* DC voltage at its input. This enables the economy of two isolated sensors.

4.3.3. *Rotor flux estimator*

In vector control with rotor flux orientation, we developed a rotor flux estimator [PIE 00]. It is based on the major relations from rotor flux orientation according to axis d of reference frame (d, q):

$$\left[1+T_{\mathrm{r}}\frac{\mathrm{d}}{\mathrm{d}t}\right]\Phi_{\mathrm{rd}}=M_{\mathrm{sr}}i_{\mathrm{sd}} \qquad \text{and} \qquad T_{\mathrm{em}}=P\frac{M_{\mathrm{sr}}}{L_{\mathrm{r}}}\Phi_{\mathrm{rd}}i_{\mathrm{sq}}$$
$$\frac{\mathrm{d}}{\mathrm{d}t}\rho=\omega+\frac{M_{\mathrm{sr}}i_{\mathrm{sq}}}{T_{\mathrm{r}}\Phi_{\mathrm{rd}}} \qquad \text{and} \qquad \rho=\int\omega_{\mathrm{mr}}\,\mathrm{d}t \qquad [4.26]$$

where ω_{mr} is the rotation speed of the rotor flux vector in relation to stator ($\omega_{\mathrm{mr}} = \omega_{\mathrm{d/s}}$) and ρ is the angular position of the flux vector or axis d in relation to phase 1 of the stator. The principle diagram of this estimator is illustrated in Figure 4.3. Angle ρ, which sets the transformation of coordinates to obtain components i_{sd}, i_{sq}, is estimated from these same components.

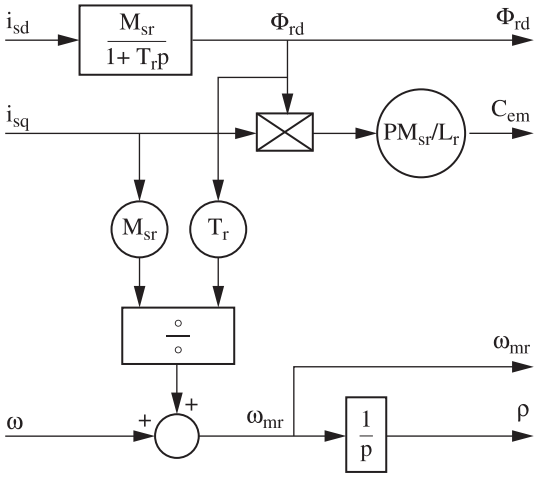

Figure 4.3. *Principle diagram of the rotor flux estimator*

In addition, rotor time constant T_{r}, variable with temperature, is directly involved in the expression of ω_{mr}, and thus the angle. Incorrect knowledge of the rotor time constant has all the more influence as the machine works at slow speed and strong torque, because the part of the second term in the expression of ω_{mr} becomes predominant. Incorrect knowledge of T_{r} leads to inaccuracy in ρ and a loss of natural decoupling obtained by the rotor flux orientation. In these conditions,

the flux is not oriented along axis d; there is a component based on q, and the flux amplitude becomes dependent on i_{sq} and thus the torque.

4.4. Flux observation

4.4.1. *Full order deterministic observer*

4.4.1.1. *Principle*

Consider an induction machine powered by a two-level Pulse Width Modulation (PWM) voltage inverter. We make a few hypotheses to simplify the model:

– We suppose that the feeding of the machine is reduced to the application of the first harmonic signals with variable amplitude and frequency. We ignore the effect of harmonics and delays caused by the inverter.

– We suppose that the rotation speed is a slow variable parameter in relation to currents and fluxes, as was explained in section 4.2.

In these conditions, the electrical machine model is linear and can be represented by a four order state system, as we have seen previously:

$$\frac{\mathrm{d}}{\mathrm{d}t} X = A \cdot X + B \cdot U \quad \text{and} \quad Y = C \cdot X \qquad [4.27]$$

where X is the state vector, U the input vector, Y the output vector, and A, B, and C are system matrices.

In a stationary reference frame, the locations of machine poles (eigenvalues of the dynamic matrix A) according to speed have the same form as the one shown in Figure 4.4. In a rotating reference frame, the location of poles according to speed is shown in Figure 4.5.

The estimator has a state model similar to that of the machine, with the same matrices A, B, and C. However, the vectors are differentiated: X^* and Y^*. The drive system and estimator are fed by the same input vector U:

$$\frac{\mathrm{d}}{\mathrm{d}t} X^* = A \cdot X^* + B \cdot U \quad \textit{and} \quad Y^* = C \cdot X^* \qquad [4.28]$$

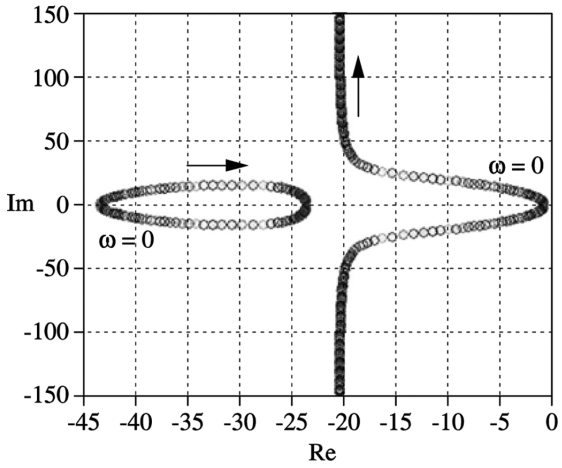

Figure 4.4. *Evolution of induction machine poles in a stationary reference frame*

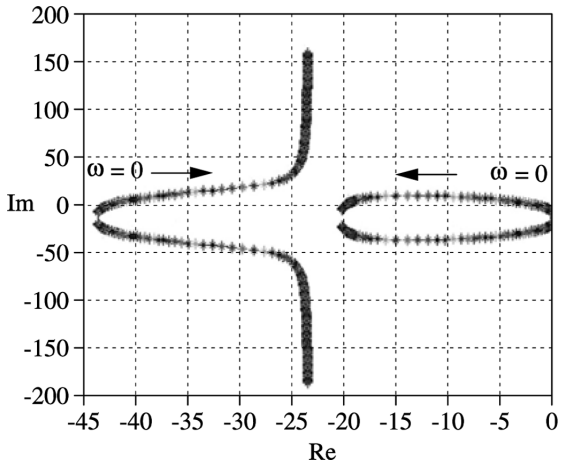

Figure 4.5. *Open loop system poles in a reference frame linked to the rotor*

In terms of an estimator, the observer evaluates the error between a measured variable and the same variable, but estimated. This error is amplified by a gain and reinjected to force the observer to converge toward a zero error. The variable used is generally the stator current vector. The principle diagram of the observer associated with an induction machine speed drive is shown in Figure 4.6.

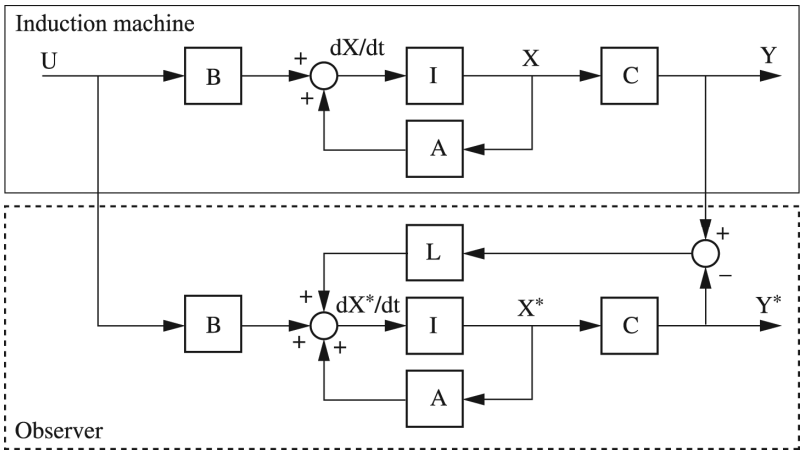

Figure 4.6. *Diagram of a deterministic state observer associated with an induction machine*

In the state transition matrix A, two parameters, rotation speed ω and reference frame speed $\omega_{d/s}$, emerge. As it is natural to consider that the rotation speed is a slow parameter, it is more difficult for speed $\omega_{d/s}$ generally linked to an electrical angular frequency. Consequently, the most appropriate choice is to use a set reference with $\omega_{d/s} = 0$.

Since the error is calculated from measurable stator currents, we must also retain stator currents as state vector components. To simplify, we can represent complex state equations. In order to do this, we define the complex vectors as:

$$X_c = \left[I_{sc}, \Phi_{rc}\right], \quad U_c = \left[V_{sc}\right], \quad \text{and} \quad Y_c = \left[I_{sc}\right]$$

with

$$I_{sc} = i_{sd} + ji_{sq} \qquad \Phi_{rc} = \Phi_{rd} + j\Phi_{rq} \qquad V_{sc} = V_{sd} + jV_{sq}$$

The complex state equation is:

$$\frac{d}{dt} X_c = A_c X_c + B_c U_c \quad \text{and} \quad Y_c = C_c X_c \qquad [4.29]$$

with

$$A_c = \begin{bmatrix} a_1 & b_1\left(\frac{1}{T_r} - j\omega\right) \\ c_1 & -\frac{1}{T_r} + j\omega \end{bmatrix} \qquad B_c^t = \begin{bmatrix} a & 0 \end{bmatrix} \qquad C_c = \begin{bmatrix} 1 & 0 \end{bmatrix}$$

where

$$a_1 = -\left[aR_s + b(1-\sigma)R_r\right] \qquad b_1 = c \qquad c_1 = cR_r$$

4.4.1.2. *State equation of the observer*

As was discussed previously, the estimator matrices and input vector are the same as those of the machine:

$$\frac{d}{dt}X_c^* = A_c X_c^* + B_c U_c \qquad Y_c^* = C_c X_c^* \qquad [4.30]$$

The error on the output vector is

$$e_c = Y_c - Y_c^*$$

and in closed loop, the observer equation becomes:

$$\frac{d}{dt}X_c^* = (A_c - L_c C_c)X_c^* + B_c U_c + L_c Y_c \qquad [4.31]$$

The new state matrix defining the dynamic of the observer is

$$A_c' = A_c - L_c C_c \qquad [4.32]$$

The determination of gain matrix L_c is done according to the desired dynamic for the observer:

$$L_c = \begin{bmatrix} L(1) \\ L(2) \end{bmatrix} \qquad [4.33]$$

Because of matrix symmetries A that we want to reproduce on matrix A', the real gain matrix L will be in the form:

$$L = \begin{bmatrix} L_1 & L_2 & L_3 & L_4 \\ -L_2 & L_1 & -L_4 & L_3 \end{bmatrix}^{\mathrm{T}} \quad \text{and} \quad L(1) = L_1 + jL_2 \qquad L(2) = L_3 + jL_4 \tag{4.34}$$

4.4.1.3. *Observability*

It is important to verify the field of observability of the observer [SIA 92]. In order to do this, we assume $\omega_a = 0$. The observability matrix is

$$\mathrm{OB}_c^t = \left[C_c, C_c A_c, \ldots, C_c A_c^{n-1} \right] \tag{4.35}$$

where n is the dimension of state vector X_c^*, that is, in this case $n = 2$. Hence:

$$\mathrm{OB}_c = \begin{bmatrix} C_c \\ C_c A_c \end{bmatrix} = \begin{bmatrix} 1 & 0 \\ a & b\left(\dfrac{1}{T_r} - \mathrm{j}\omega\right) \end{bmatrix} \tag{4.36}$$

$$\text{with} \quad a_1 = -\frac{1}{\sigma T_s} - \frac{1-\sigma}{\sigma T_r} \quad \text{and} \quad b_1 = \frac{1-\sigma}{\sigma M_{sr}}$$

$$\det(\mathrm{OB}) = \det(\mathrm{OB}_c) \times \det(\overline{\mathrm{OB}}_c) = b_1^2 \left[\frac{1}{T_r^2} + \omega^2 \right] \tag{4.37}$$

We observe that, regardless of velocity, the determinant det(OB) is not zero, and consequently, the condition of observability is fully respected for any operation point.

4.4.1.4. *Calculation of observer gain*

The determination of gain matrix L_c is done by imposing closed loop observer poles in relation to the solution machine poles of

$$\det(pI - A_c) = 0$$

These poles are generally complex, two by two, and each pair describes a location according to velocity. In the large field of speed, both locations are far enough apart (Figure 4.4) that we can distinguish between the poles connected to stator current (the fastest ones) and those connected to the flux (the slowest). The choice for gain matrix will consist in accelerating the poles linked to the flux. Empirically, this acceleration is a compromise between velocity and stability, and it is possible, for example, to multiply, by a factor of 3 or 4, the real part of the poles corresponding to the slowest modes. Several solutions can be considered to account for the rotation speed:

– the gain matrix is maintained as a constant, the poles then describe a location that must be verified to make sure they still correspond to a satisfying response;

– or the gain matrix is variable with speed in order to maintain constant poles. We choose to evolve the gains, in intervals and not continuously, according to this rotation speed.

When the first solution is chosen, matrix factors L_c are defined and coefficients β_1 and β_2 are a function of the rotation speed:

$$\det(pI - A'_c) = p^2 + \beta_1 p + \beta_2$$

By identifying:

$$\beta_1 = L(1) - a_1 + \frac{1}{T_r} - j\omega \quad \text{and} \quad \beta_2 = \left[L(1) - a_1 + b_1(L(2) - c_1)\right]\left[\frac{1}{T_r} - j\omega\right] \quad [4.38]$$

We deduce $L(1)$ and $L(2)$ values according to rotation speed and the four gains of gain matrix L. In Figure 4.7, pole locations of the open loop system and observer are indicated. A simulation result is shown in Figure 4.8, from an initial error on the estimated flux [SIA 92].

4.4.1.5. *Example of observer robustness*

In state matrix A, rotor resistance R_r occurs in several terms. This resistance is generally not well known because of rotor measure problems, and it varies in large proportions with temperature and pellicular effect on the rotor cage. From an initial value R_{r0}, we represent its variations by ΔR_r. Corresponding to the initial resistance value, we call state matrix A'_{c0} and corresponding state vector X^*_{c0}.

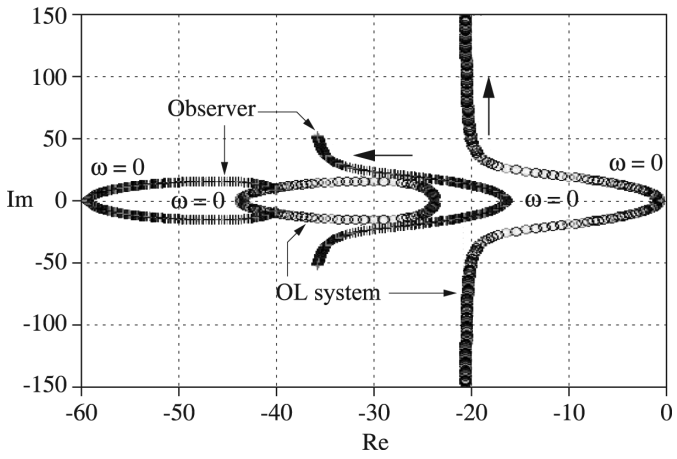

Figure 4.7. *Pole locations of the system and observer after the determination of* β_1 and β_2

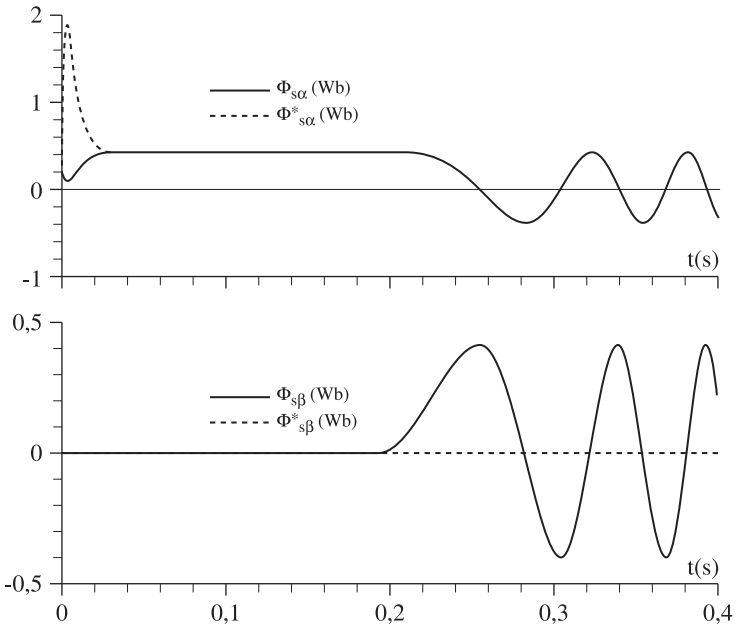

Figure 4.8. *Simulation results of the convergence of the flux deterministic observer*

The state equation becomes:

$$\frac{\mathrm{d}}{\mathrm{d}t}\left[X_{\mathrm{c0}}^{*}+\Delta X_{\mathrm{c}}^{*}\right]=\left[A'_{\mathrm{c0}}+A_{\Delta}\,\Delta R_{\mathrm{r}}\right]\left[X_{\mathrm{c0}}^{*}+\Delta X_{\mathrm{c}}^{*}\right]+B_{\mathrm{c}}U_{\mathrm{c}}+L_{\mathrm{c}}C_{\mathrm{c}}X_{\mathrm{c0}}$$

$$A'_{\mathrm{c0}}=\begin{bmatrix} a_{10}-L(1) & b_1\left(\dfrac{1}{T_{\mathrm{r0}}}-\mathrm{j}\omega\right) \\ c_{10}-L(2) & -\dfrac{1}{T_{\mathrm{r0}}}+\mathrm{j}\omega \end{bmatrix} \qquad A_{\Delta}=\begin{bmatrix} -\dfrac{1-\sigma}{\sigma L_{\mathrm{r}}} & \dfrac{b}{L_{\mathrm{r}}} \\ \dfrac{M_{\mathrm{sr}}}{L_{\mathrm{r}}} & -\dfrac{1}{L_{\mathrm{r}}} \end{bmatrix} \qquad [4.39]$$

Robustness will be characterized by the relation:

$$A'_{\mathrm{c0}}\,\Delta X_{\mathrm{c}}^{*}=-A_{\Delta}X_{\mathrm{c0}}^{*}\,\Delta R_{\mathrm{r}} \qquad [4.40]$$

By ignoring the second order terms, the above state equation is written as

$$\frac{\mathrm{d}}{\mathrm{d}t}X_{\mathrm{c}}^{*}=A'_{\mathrm{c}}X_{\mathrm{c}}^{*}+A_{\Delta}X_{\mathrm{c0}}^{*}\,\Delta R_{\mathrm{r}}+B_{\mathrm{c}}U_{\mathrm{c}}+L_{\mathrm{c}}C_{\mathrm{c}}X_{\mathrm{c}} \qquad [4.41]$$

To improve observer robustness, a technique consists of increasing its order by using resistance variation ΔR_{r} as new variable that we use as state equation:

$$\frac{\mathrm{d}}{\mathrm{d}t}\left[\Delta R_{\mathrm{r}}\right]=0 \quad \text{and} \quad A_{\Delta}X_{\mathrm{c0}}^{*}\,\Delta R_{\mathrm{r}}=\begin{bmatrix} b_1 \\ -1 \end{bmatrix}I_{\mathrm{r0}}^{*}\,\Delta R_{\mathrm{r}}=B_{\mathrm{p}}\,\Delta R_{\mathrm{r}} \qquad [4.42]$$

If L_{p} is the gain corresponding to this new state variable, then the equation becomes:

$$\begin{aligned} &\frac{\mathrm{d}}{\mathrm{d}t}\begin{bmatrix} X_{\mathrm{c}}^{*} \\ \Delta R_{\mathrm{r}} \end{bmatrix}=\begin{bmatrix} A'_{\mathrm{c0}} & B_{\mathrm{p}} \\ -L_{\mathrm{p}} & 0 \end{bmatrix}\begin{bmatrix} X_{\mathrm{c}}^{*} \\ \Delta R_{\mathrm{r}} \end{bmatrix}+B_{\mathrm{G}}U_{\mathrm{c}}+L_{\mathrm{G}}C_{\mathrm{G}}X_{\mathrm{c}} \\ &B_{\mathrm{G}}^{\mathrm{t}}=\begin{bmatrix} \dfrac{1}{\sigma L_{\mathrm{s}}} & 0 & 0 \end{bmatrix} \qquad L_{\mathrm{G}}^{\mathrm{t}}=\begin{bmatrix} L(1) & L(2) & L_{\mathrm{p}} \end{bmatrix} \qquad C_{\mathrm{G}}=\begin{bmatrix} 1 & 0 & 0 \end{bmatrix} \end{aligned} \qquad [4.43]$$

This approach consists of adding a rotor resistance observer associated with the flux observer, according to the diagram in Figure 4.9.

We have carried out step variations in the rotor resistance (Figure 4.10), which is unrealistic, and we compared by simulation the results obtained with the disturbance observer in relation to those with the state observer only. We verify the advantage of this resistance estimation that can also be used to adapt machine control.

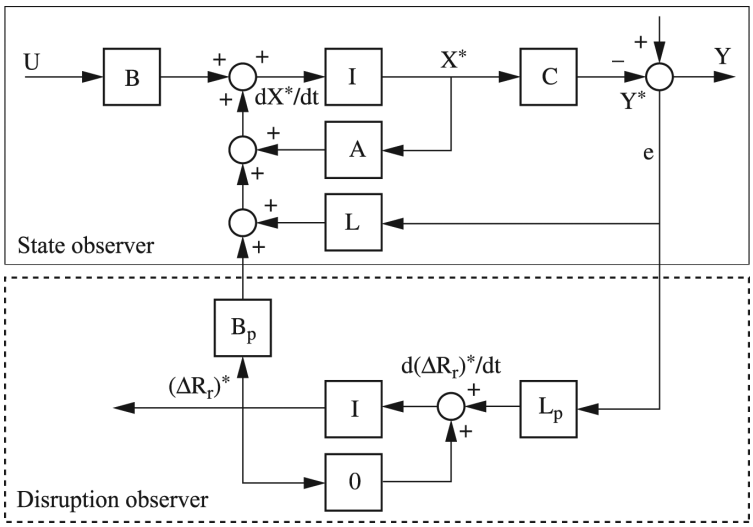

Figure 4.9. *Flux state observer and disturbance observer*

4.5. Linear stochastic observers – Kalman–Bucy filters

4.5.1. *Introduction*

The adoption of a deterministic approach for the state estimation of a physical system ignores the notions of uncertainty and random fluctuations. They are linked to errors and noises inherent to any physical system, as well as to noises marring power signals caused by static converters. When the level of noise is low, the deterministic approach can turn out to be enough, but in other cases, the consideration of the stochastic aspect enables us to increase the precision of estimated variables.

In this approach, there is a very precise link between estimator pole placement and statistic noise parameters. In fact, because of the noise description, matrix choice K of Kalman gains is optimal in the sense of the minimal variation of estimated values. The basic structure of a stochastic estimator is similar to that of a closed loop deterministic state observer. The Kalman–Bucy filter is a recursive algorithm of data processing, generating the estimate of state variables of a dynamic system from a series of measures marred by noises.

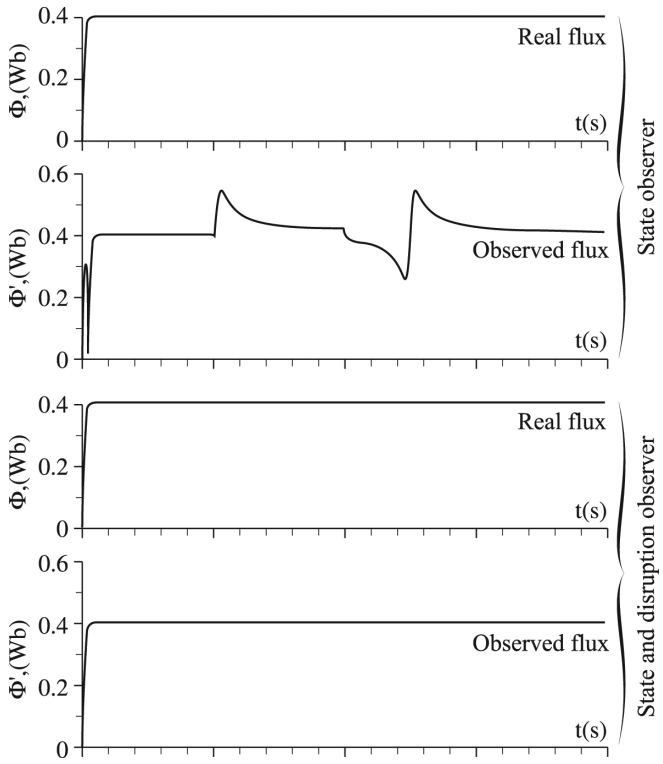

Figure 4.10. *Observation of the flux with or without disruption observer during the variations of rotor resistance*

4.5.2. *Kalman–Bucy filter model*

In terms of the deterministic model, the filter model contains two additional terms $b_{sn}(t)$ and $b_{mn}(t)$, respectively, state noises and measuring noises:

$$\frac{\mathrm{d}}{\mathrm{d}t}X^* = AX^*(t) + BU(t) + b_{sn}(t) \qquad Y^*(t) = CX^*(t) + b_{mn}(t) \qquad [4.44]$$

As previously, we choose a stationary reference frame $\alpha_s\beta_s$ and vectors X^*, Y^* and U are

$$X^*(t) = \begin{bmatrix} i^*_{s\alpha} & i^*_{s\beta} & \Phi^*_{r\alpha} & \Phi^*_{r\beta} \end{bmatrix}^{\mathrm{T}} \qquad Y^*(t) = \begin{bmatrix} i^*_{s\alpha} & i^*_{s\beta} \end{bmatrix}^{\mathrm{T}}$$
$$U(t) = \begin{bmatrix} V_{s\alpha} & V_{s\beta} \end{bmatrix}^{\mathrm{T}} \qquad [4.45]$$

Noises must have the following statistic properties:

– average value or mathematical esperance is equal to zero:

$$E\left[b_{\mathrm{rs}}(t)\right] = E\left[b_{\mathrm{rm}}(t)\right] = 0$$

– autocorrelation form as below:

$$E\left[b_{\mathrm{rs}}(t)\cdot b_{\mathrm{rs}}(t)^{\mathrm{T}}\right] = Q(t)\delta(t-\tau) \quad \text{and} \quad E\left[b_{\mathrm{rm}}(t)\cdot b_{\mathrm{rm}}(t)^{\mathrm{T}}\right] = R(t)\delta(t-\tau)$$

– absence of correlation between noises:

$$E\left[b_{\mathrm{rm}}(t)\cdot b_{\mathrm{rs}}(t)^{\mathrm{T}}\right] = 0$$

– absence of correlation between noises and initial state:

$$E\left[b_{\mathrm{rm}}(t)\cdot X(t_0)^{\mathrm{T}}\right] = E\left[b_{\mathrm{rs}}(t)\cdot X(t_0)^{\mathrm{T}}\right] = 0$$

$\delta(u)$ is a pulse function of Dirac, matrices $Q(t)$ and $R(t)$ are symmetrical, defined non-negative and represent spectral densities with average noise power. The discretization of the state equation above with a sampling period T_{S} is:

$$\begin{aligned} X^*(k) &= \phi_a(k,k-1)X^*(k-1) + \phi_b(k,k-1)U(k-1) + b_{\mathrm{rs}}(k) \\ Y^*(k) &= \phi_c(k)X^*(k) + b_{\mathrm{rm}}(k) \end{aligned} \qquad [4.46]$$

We define state transition matrices ϕ_a and ϕ_b between instants $(k-1)T_{\mathrm{S}}$ and kT_{S}:

$$\begin{aligned} \phi_a(k,k-1) &= \exp\left[\int_{(k-1)T_{\mathrm{S}}}^{kT_{\mathrm{S}}} A(\tau)\mathrm{d}\tau\right] \\ \phi_b(k,k-1) &= \exp\left[\int_{(k-1)T_{\mathrm{S}}}^{kT_{\mathrm{S}}} \phi_a(t,\tau)\cdot B\cdot U(\tau)\mathrm{d}\tau\right] \\ \phi_c(k) &= C \\ Q(k) &= E\left[b_{\mathrm{sn}}(k)\cdot b_{\mathrm{sn}}(k)^{\mathrm{T}}\right] \quad \text{and} \quad R(k) = E\left[b_{\mathrm{mn}}(k)\cdot b_{\mathrm{mn}}(k)^{\mathrm{T}}\right] \end{aligned} \qquad [4.47]$$

In practice, matrices ϕ_a and ϕ_b are approximated by limited developments:

$$\phi_a(k,k-1) = \sum_{n=0}^{n=n'} \frac{[T_s A(\omega)]^n}{n!} \quad \text{and} \quad \phi_b(k,k-1) = \sum_{n=0}^{n=n'} \frac{[T_s B(\omega)]^n}{n!} \qquad [4.48]$$

In general, we limit the development of ϕ_a at order two maximum and that of ϕ_b at order one, or:

$$\begin{aligned} \phi_a(k,k-1) &= I_4 + T_s \cdot A(\omega) + \frac{1}{2}[T_s \cdot A(\omega)]^2 \\ \phi_b(k,k-1) &= T_s[I_4 + \frac{T_s}{2} A(\omega)]B \\ Q(k) &= T_s \cdot \phi_a(k,k-1) Q_0 \cdot \phi_a{}^{T}(k,k-1) \quad \text{and} \quad R(k) = R_0 I_2 \end{aligned} \qquad [4.49]$$

Q_0 is a rank four diagonal matrix with terms that are the initial values of covariances. I_2 and I_4 are rank two and four unit matrices. Matrices R_0 and Q_0 play an important role in the convergences of the Kalman filter, and we should define them well.

The filter algorithm (Figure 4.11) contains a prediction and a correction part. The general diagram of the discretized filter is shown in Figure 4.12.

4.5.3. *Convergence of the Kalman filter*

If covariance matrices $P(k,k)$ are no longer defined as positive, then the filter can diverge. This situation can be a result of inaccuracies linked to discretization and numeric precision. Negative terms can then emerge on the major diagonal of $P(k,k)$.

The precision problem guides the choice for the microprocessor used for the implementation of the filter's algorithm. It was proven that a 32-bit floating point RISC architecture is very well adapted for obtaining sufficient precision [BEN 93].

An analysis of the Kalman gain matrix shows that it has the following form:

$$K(k,k) = \begin{bmatrix} k_{11}(k,k) & k_{12}(k,k) \\ -k_{12}(k,k) & k_{11}(k,k) \\ k_{13}(k,k) & k_{14}(k,k) \\ -k_{14}(k,k) & k_{13}(k,k) \end{bmatrix} \qquad [4.50]$$

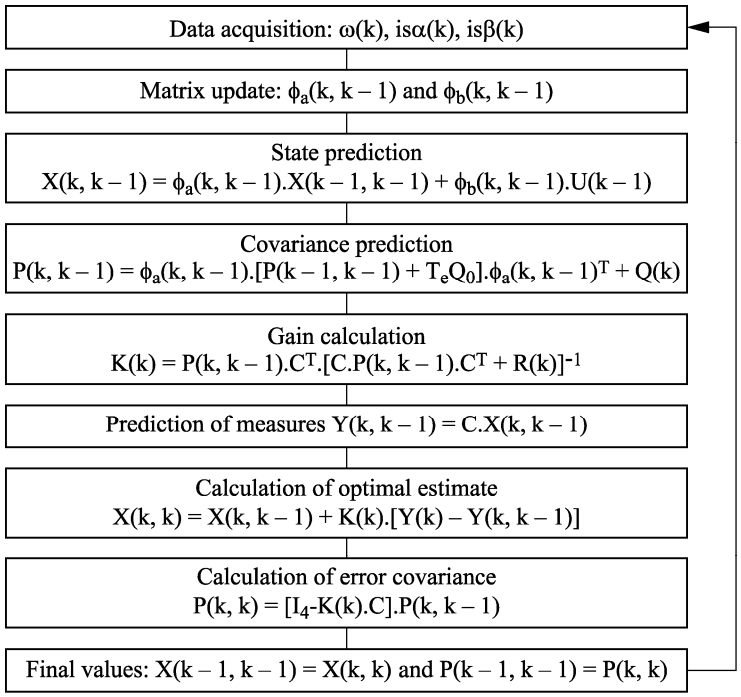

Figure 4.11. *Kalman filter algorithm*

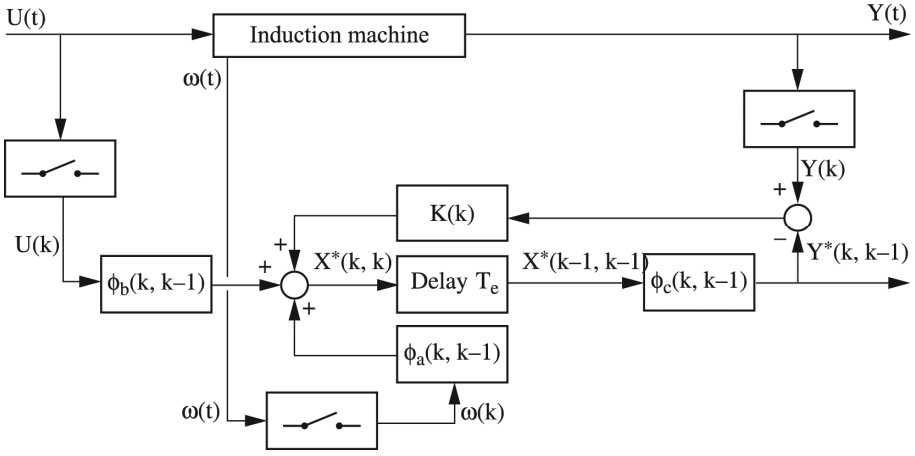

Figure 4.12. *General diagram of the Kalman filter for an induction machine*

The elements of this matrix are functions of the machine's rotation speed. The evolution of gains $k_{11}(k, k)$ and $k_{12}(k, k)$ according to the speed variation is shown in Figure 4.13. In addition, the definition of gain matrix $K(k,k)$ and the covariance matrix of estimation error $P(k,k)$ does not depend on the knowledge of measures $Y(k)$. We can therefore store the values of Kalman gains in tables and obtain shorter calculation times.

We have seen previously that matrices $Q(k)$ and $R(k)$ depend on their initial values Q_0 and R_0. The choice of these initial values greatly conditions the operation of the Kalman filter. There is no direct method for defining them. Authors developed real-time adaptation algorithms based on the quality of estimation. But Q_0 and R_0 become state variables, thus increasing the state vector order and corresponding calculation times. We can also define these covariances by trial and error method with the help of consecutive simulations. We can, for example, choose [JAC 95]:

$$Q_0 = \begin{bmatrix} \alpha & 0 & 0 & 0 \\ 0 & \alpha & 0 & 0 \\ 0 & 0 & \beta & 0 \\ 0 & 0 & 0 & \beta \end{bmatrix} \quad \text{and} \quad R_0 = \begin{bmatrix} \gamma & 0 \\ 0 & \gamma \end{bmatrix} \qquad [4.51]$$

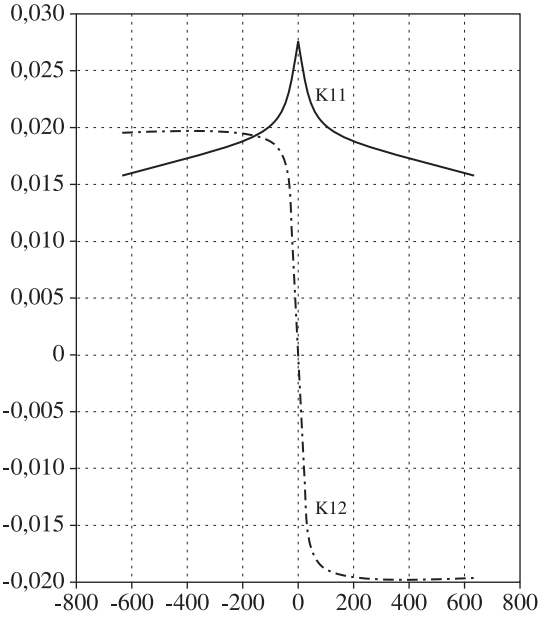

Figure 4.13. *Examples of the variations of two Kalman gain matrix factors*

Where α, β and γ are defined within a constant. We have two degrees of freedom:

– α_1 relation between state noises and measuring noises; and

– α_2 relation between flux and current state noises.

$$Q_0 = \alpha_1 \begin{bmatrix} 1 & 0 & 0 & 0 \\ 0 & 1 & 0 & 0 \\ 0 & 0 & \alpha_2 & 0 \\ 0 & 0 & 0 & \alpha_2 \end{bmatrix} \quad \text{and} \quad R_0 = \begin{bmatrix} 1 & 0 \\ 0 & 1 \end{bmatrix} \qquad [4.52]$$

Factors α_1 and α_2 are defined empirically and by a certain number of simulations.

4.5.4. *Simulation results and experimental results*

In order to test this filter in simulation, it was necessary to generate measuring noises in stator currents $i_{s\alpha}$ and $i_{s\beta}$. This was done by the generation of two random numbers N_α and N_β. Simulations were done on a 45 kW machine, which injects with a 10% measuring noise in relation to the rated current [BEN 93].

In Figure 4.14, the comparative results of real and estimated dimensions on rotor flux components $\Phi_{r\alpha}$ and $\Phi_{r\beta}$, the two-phase flux module F_r, and the phase of this flux Θ_Φ are shown.

We verify the correct performances of the filter, despite the rate of noises on measures, during the establishment of the flux before machine startup.

Experimental tests are done on an induction variable speed drive with a metallurgical application and power of 90 kVA, made up of a Gate Turn-Off Switch (GTO) voltage inverter associated on the continuous side to a rectifier and a filter, a 45-kW induction machine, a vector control defining the voltage provided by the inverter to the machine stator, and a Kalman filter for estimating the rotor flux. The variable speed drive has a speed sensor.

The general diagram of this variable speed drive is shown in Figure 4.15. Two experimental tests, corresponding to a reversal of the rotation direction (Figure 4.16) and an abrupt variation of the load torque (Figure 4.17) show the performances of this variable speed drive [BEN 93].

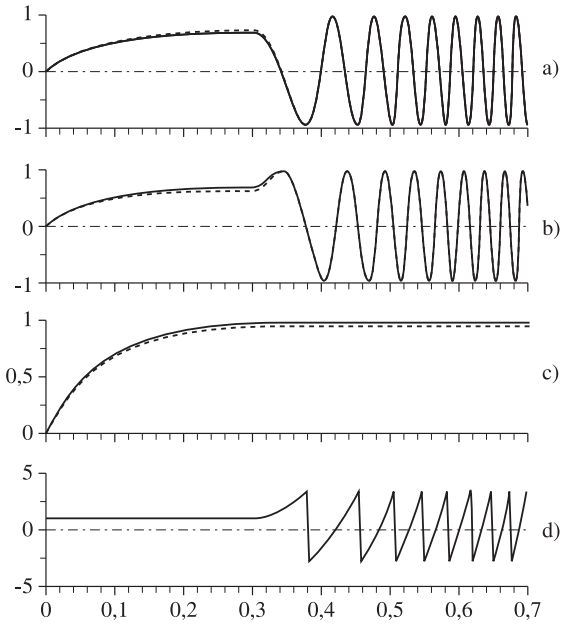

Figure 4.14. *Comparison of real and estimated fluxes by the Kalman filter during machine magnetizing*

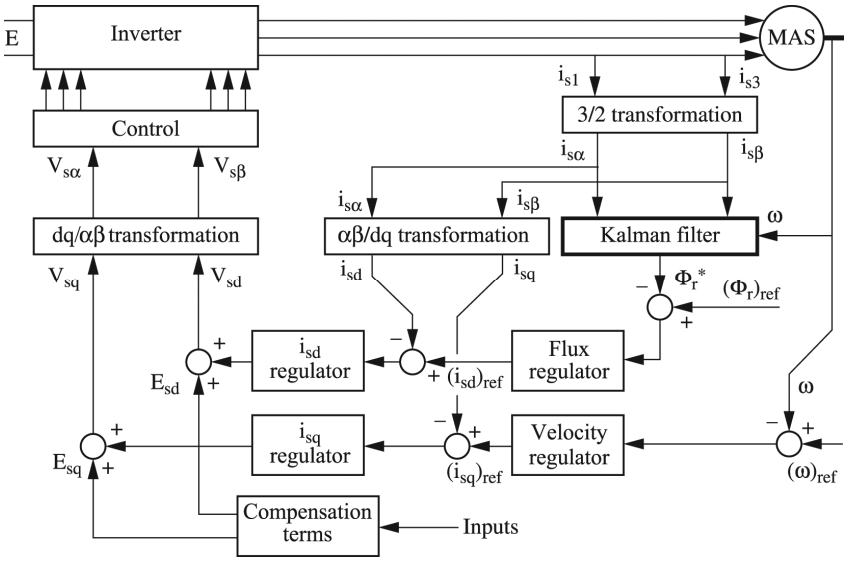

Figure 4.15. *General diagram of the variable speed drive with vector control and Kalman filter*

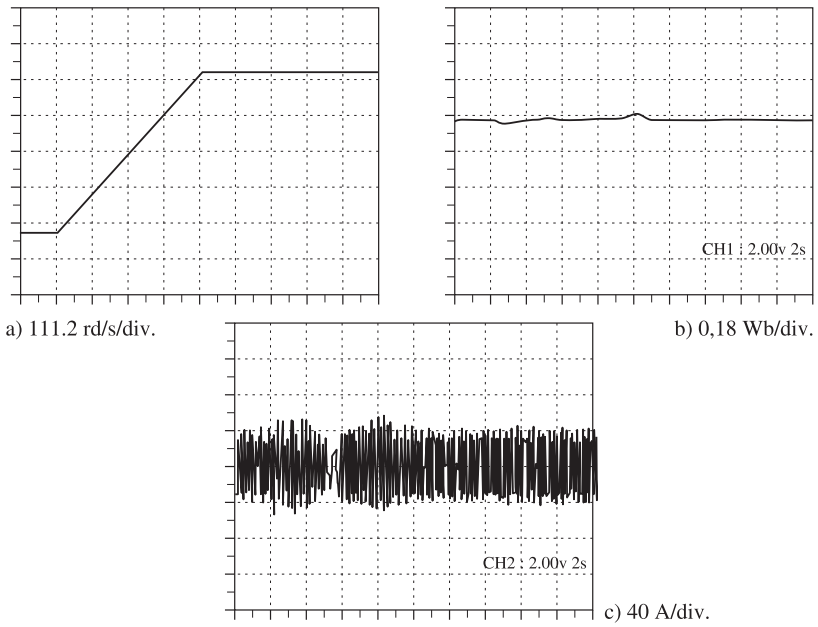

Figure 4.16. *Experimental test–reversal of the rotation direction*

Other experimental tests were carried out on the prototype of a chain of an induction traction of high-speed train (TGV). This prototype corresponds to a 300-kW motor with a nominal torque of 2,100 Nm. We are dealing with torque control without any speed regulation [JAC 95].

Figure 4.18 shows a series of accelerations and brakes with a representation of the variation of the continuous input voltage (catenary) U_c, the current in a stator, and real electromagnetic torque phase compared to the reference torque. The first acceleration occurs at the same time as motor magnetizing, leading to a relatively slow torque ascent.

In Figures 4.19 and 4.20, a reference torque cycle and the real response for two speeds, one close to stopping and average speed, are shown.

In Figures 4.21-4.23, we present the experimental responses to the torque set point profile (Figure 4.19) for several coefficient couples α_1 and α_2 [4.52] and for two different speeds, practically stopped and average speed.

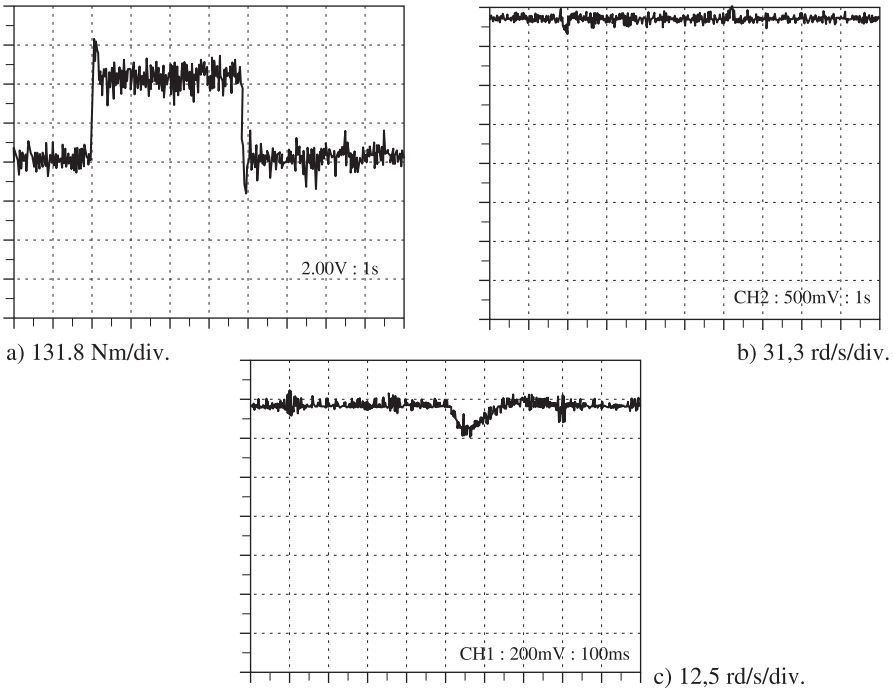

Figure 4.17. *Experimental test–impact of the load torque*

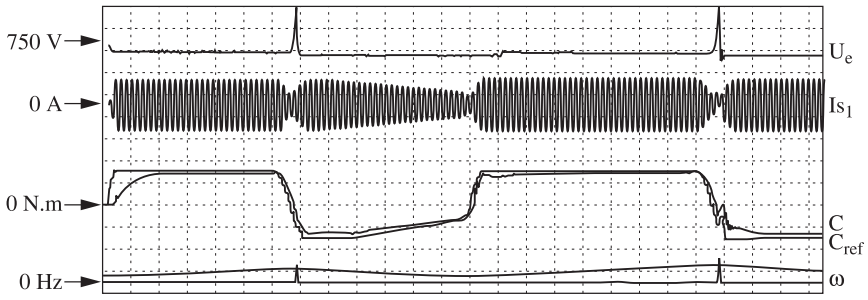

Figure 4.18. *Traction and braking cycle for a railway chain*

We can comment these tests as follows. Figure 4.21 ($\alpha_1 = 10^4$ and $\alpha_2 = 2.5 \times 10^{-8}$): at low speed, the torque is not well regulated, there are over shoots and static errors. The torque response is very oscillatory. At higher speed, the behavior is perfectly fine. Torque ramps and steps are well followed.

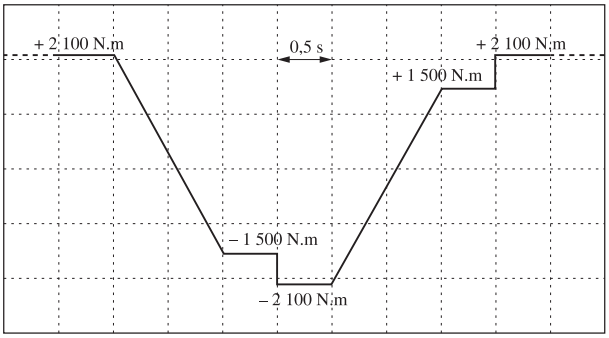

Figure 4.19. *Torque set point cycle*

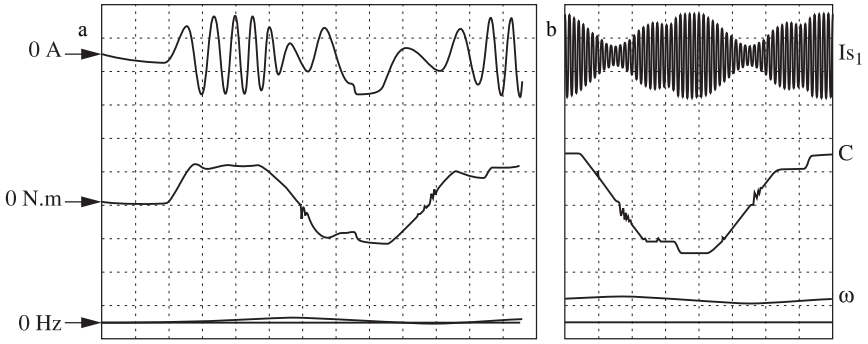

Figure 4.20. *Electromagnetic torque, speed, and stator current cycle (a) zero speed; (b) average speed*

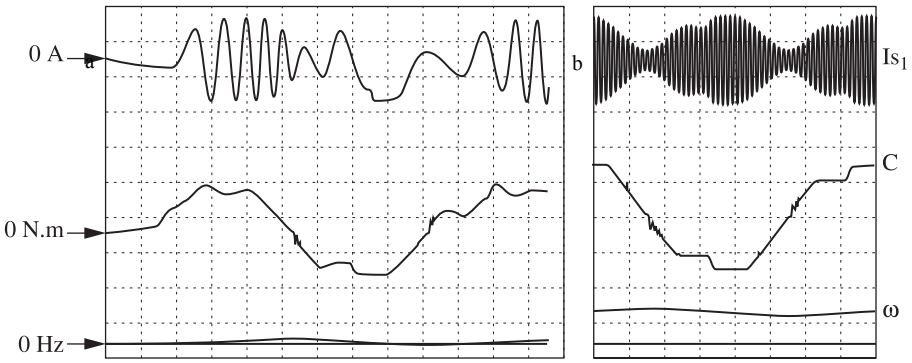

Figure 4.21. *Electromagnetic torque, speed, and stator current (a) zero speed, (b) average speed* $\alpha_1 = 10^4$ *and* $\alpha_2 = 2.5 \times 10^{-8}$

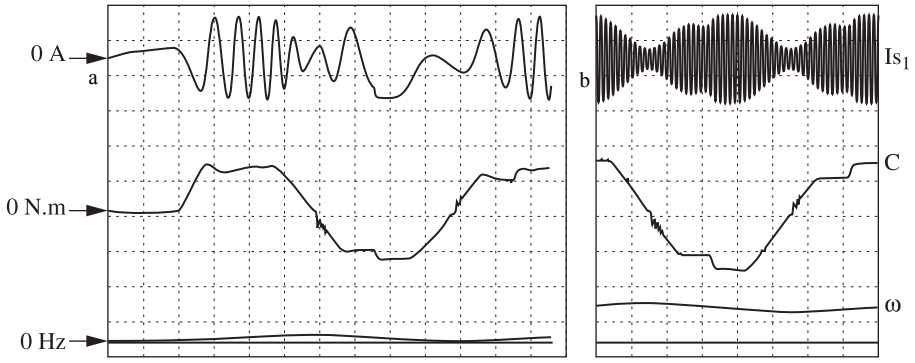

Figure 4.22. *Electromagnetic torque, speed and stator current (a) zero speed (b) average speed* $\alpha_1 = 1.6.10^3$ *and* $\alpha_2 = 10^{-7}$

Figure 4.22 ($\alpha_1 = 1.6 \times 10^3$ and $\alpha_2 = 10^{-7}$): we do not trust the state model in relation to current measures as much as the state flux model in relation to the current state model. The results are clearly better. At low speed, torque ramps and steps are better followed than in the previous case. But a few over shoots and errors remain.

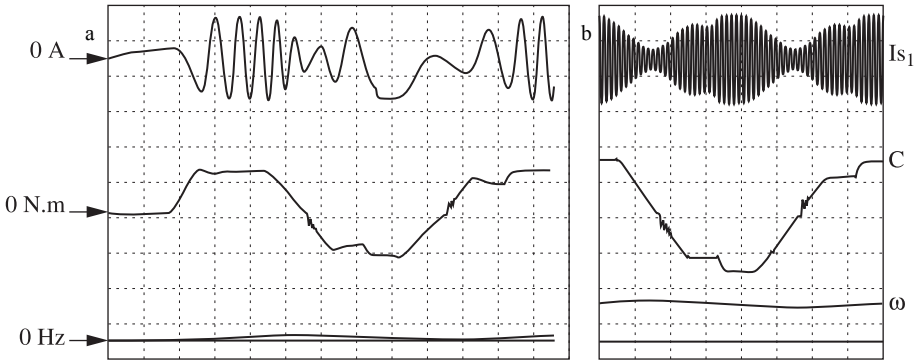

Figure 4.23. *Electromagnetic torque, speed, and stator current (a) zero speed, (b) average speed* $\alpha_1 = 10^3$ *and* $a_2 = 2.5 \times 10^{-8}$

Figure 4.23 ($\alpha_1 = 10^3$ and $\alpha_2 = 2.5 \times 10^{-8}$): compared to the first test, we trust less the state model in relation to current measures. The results obtained are very close to those in the second case. We verify that the first torque over shoot is lower than in the second case.

In conclusion, adjusting the observer does not have a significant impact in average or high-speed operations. The system is much more difficult to control at low speed. The adjustment of two factors must be done at very slow speed.

4.6. Separate estimation and observation structures of the rotation speed

4.6.1. *Introduction*

Control without mechanical sensor creates great interest in all range power of variable speed drives. For low-power variable speed drives, the cost and encumbrance of the speed sensor were prohibitive compared to those of the variable speed drive. In addition, many low-power applications do not require precise knowledge of the speed. For high-power motors, the sensor cost is not the first concern; instead we speak of problems linked to its assembly and maintenance. There is not always a machine shaft end available for the speed sensor. In addition, on high-power equipment, axial movements and vibrations deteriorate the sensor and its coupling, as well as the quality of speed measures.

In order to obtain good performances from variable speed drives, especially at very low speeds and large loads, knowledge of speed is necessary.

All these considerations lead to replacing the speed sensors by estimators or observers.

In this section, we present a certain number of speed estimation systems associated with estimators or flux observers, but separate from them [FOR 96]. In Chapter 3, non-linear observers were disscused where flux and speed are estimated in the same algorithm.

4.6.2. *General principles*

They are organized around three main concerns:

– the choice of the model: there is a compromise between a simple model, generally not precise, but not very dependent on parameters, and a more complex and often less robust model than parametric variations;

– the precision of parameters: resistive parameters are mainly the ones that will have a predominant influence at very low speeds and large loads. In particular, natural decoupling in the vector control depends on the precision of the angle of transformation and thus rotor resistance;

– real-time calculation precision: this point is particularly important for controls with low sampling frequency. This corresponds to high power speed drives where the modulation frequency of the inverter is low and leads to the choice of a sampling frequency that is low, so as to take advantage of signal synchronization. In this case, there can be the introduction of delays and errors linked to the precision of the calculator.

The speed can be identified, estimated, observed, or come from an adaptive process:

– identification: the speed is determined by the real-time analysis of the influence of faults or characteristics of the machine on stator currents–mechanical out of balance, slots, or magnetic saturation. But the information obtained is generally less precise as the speed is low. Some techniques consist in triggering specific saturations or increasing some faults. But this can result in additional vibrations. These techniques are not new, but the available real-time calculation power makes them usable;

– estimation: the open loop estimation of speed uses self-piloting relations (frequency composition), often deducted from electrical equations in sinusoidal mode. Open loop operation makes these estimation techniques weak;

– observation: observation uses the mechanical model instead. We often associate the load torque to speed as a state variable of the mechanical model. It implies separation of electrical and mechanical modes;

– adaptive principle: the electrical model makes it possible to adapt the quantity that we wish to determine, speed in this case, with the help of a choice of measures and estimated variables. The problem resides in the choice of the optimizing function to obtain the speed.

4.6.3. *Speed estimation and observation methods*

4.6.3.1. *Speed calculation by the self-piloting relation*

We presume that current and flux electrical variables are estimated by an observer, for example, an order four linear Kalman filter as presented in section 4.5. If we are in the case of vector control with rotor flux orientation, then relation [4.26] results in:

$$\frac{\mathrm{d}}{\mathrm{d}t}\rho = \omega + \frac{T_\mathrm{r} i_\mathrm{sq}}{M_\mathrm{sr}\Phi_\mathrm{rd}}$$

The observer provides the rotor flux components:

$$\Phi_{r\alpha}^{*} \quad \text{and} \quad \Phi_{r\beta}^{*}$$

$$\rho^{*} = \text{arctg}\frac{\Phi_{r\beta}^{*}}{\Phi_{r\alpha}^{*}} \qquad [4.53]$$

From currents $i_{s\alpha}$ and $i_{s\beta}$ deducted from measures, estimated current i_{sq}^{*} is:

$$i_{sq}^{*} = -i_{s\alpha} \cdot \sin\rho^{*} + i_{s\beta} \cdot \cos\rho^{*} \quad \text{and} \quad \Phi_{rd}^{*} = \sqrt{\left(\Phi_{r\alpha}^{*}\right)^{2} + \left(\Phi_{r\beta}^{*}\right)^{2}}$$

The speed estimate is:

$$\omega^{*} = \frac{\mathrm{d}}{\mathrm{d}t}\left[\text{arctg}\frac{\Phi_{r\beta}^{*}}{\Phi_{r\alpha}^{*}}\right] - \frac{M_{sr} \cdot \left[-i_{s\alpha} \cdot \sin\rho^{*} + i_{s\beta} \cdot \cos\rho^{*}\right]}{T_{r}\sqrt{\left(\Phi_{r\alpha}^{*}\right)^{2} + \left(\Phi_{r\beta}^{*}\right)^{2}}} \qquad [4.54]$$

We can see with relations [4.53] and [4.54] that precision and robustness of the speed estimation mainly depend on those of the flux estimation. In addition, as was discussed previously (section 4.3.2), time constant T_r is sensitive to temperature variables.

In discrete mode with a sampling period T_s, we have:

$$\omega^{*}(n) = \frac{\rho^{*}(n) - \rho^{*}(n-1)}{T_e} - \frac{M_{sr} \cdot i_{sq}^{*}(n)}{T_r \cdot \Phi_{rd}^{*}(n)} \qquad [4.55]$$

The principle diagram of this estimation is illustrated in Figure 4.24.

The estimation of speed is in open loop, with all the drawbacks of this type of operation: static errors, lack of robustness, and possible instability. Since the estimated speed contains a term with a dynamic that is meant for electrical quantities dimensions, we must treat this term with a filter, with a bandwidth that is similar to that of the speed.

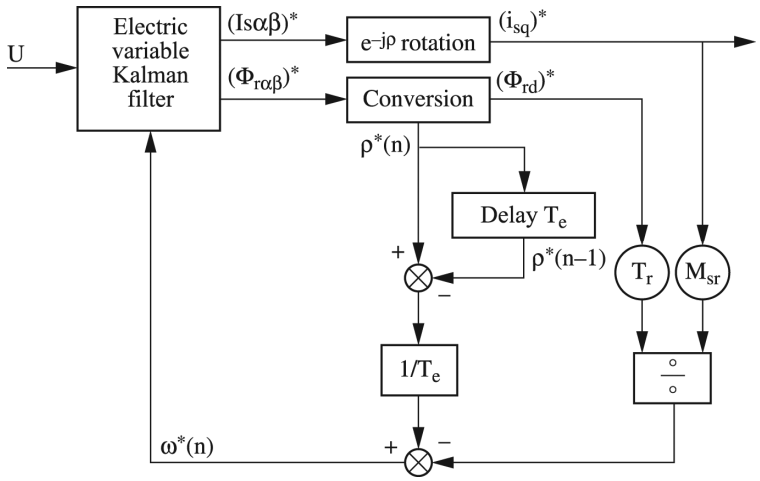

Figure 4.24. *Electric observer associated with an estimator by frequency addition*

4.6.3.2. *Association of a mechanical observer to an estimator by frequency addition*

This filtering requirement may be made by the use of an order two mechanical Kalman filter, with state variables being speed and load torque. To close the mechanical filter, we must define a measurable output vector. The load torque is generally unknown and no measure is considered. We use a pseudo-measure of speed given by the previous estimator. We then obtain the principle diagram shown in Figure 4.25. The pseudo-measure is: $\left[\omega(n)\right]_1$. The Kalman gain acts on the difference between these two quantities. The electromagnetic torque is calculated from variables estimated according to relation [4.7].

The state equations of a mechanical observer are:

$$\frac{\mathrm{d}X_{\mathrm{m}}^{*}}{\mathrm{d}t} = A_{\mathrm{m}}X_{\mathrm{m}}^{*} + B_{\mathrm{m}}U_{\mathrm{m}}^{*} + L_{\mathrm{m}}\left[Y_{\mathrm{m1}}^{*} - Y_{\mathrm{m2}}^{*}\right] \quad \text{and} \quad Y_{\mathrm{m2}}^{*} = C_{\mathrm{m}}X_{\mathrm{m}}^{*} \qquad [4.56]$$

with:

$$X_{\mathrm{m}}^{*} = \left[\omega_2^{*} \quad C_{\mathrm{r}}^{*}\right]^{t} \quad Y_{\mathrm{m2}}^{*} = \omega_2^{*} \quad Y_{\mathrm{m1}}^{*} = \omega_1^{*} \quad U_{\mathrm{m}}^{*} = C_{\mathrm{em}}^{*}$$

$$A_{\mathrm{m}} = \begin{bmatrix} -(f/J) & -(P/J) \\ 0 & 0 \end{bmatrix} \quad B_{\mathrm{m}} = \begin{bmatrix} P/J \\ 0 \end{bmatrix} \quad C_{\mathrm{m}} = \begin{bmatrix} 1 & 0 \end{bmatrix}$$

For the load torque, we have the simplest state equation:

$$\frac{\mathrm{d}}{\mathrm{d}t}C_{\mathrm{r}}^{*} = 0 \qquad [4.57]$$

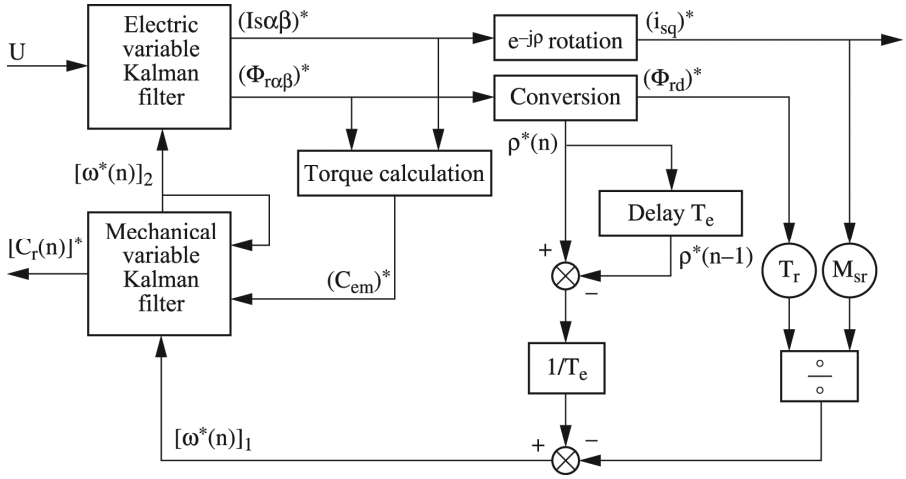

Figure 4.25. *Principle diagram of a speed estimator by frequency addition associated with a mechanical observer*

In Chapter 7 of this book, dedicated to the estimation of the load torque, the calculation of factors of matrix L_{m} is clarified.

Since the mechanical filter does not depend on any variable parameter, as is the case with speed in the electrical filter, covariances of measuring and state noises of the mechanical filter are identical, regardless of the machine's operation point.

This system is tested with the help of an operation cycle made up of:

– the establishment of the flux from 0 to 0.3 s;
– the nominal torque acceleration up to 1,200 rpm;
– the impact of a rated load from 1 to 1.8 s;
– a reversal of the rotation direction;
– braking until slow speed (190 rpm);
– the impact of a load equal to one-third of the rated load.

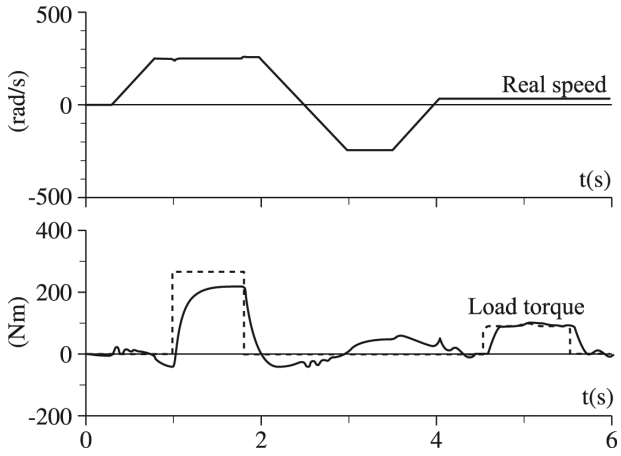

Figure 4.26. *Estimation of speed and load torque for an operation cycle*

We verify (Figure 4.26) the correct estimation of speed and load torque that can be used to compensate the load in a speed regulator.

4.6.3.3. *Adaptive mechanism (MRAS)*

This method is based on the comparison of quantities obtained in two different ways – one with a calculation that does not explicitly depend on speed (output reference model Y_r) and the other by a calculation directly depending on speed (output adaptable model Y_a).

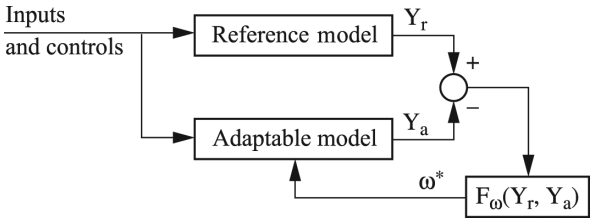

Figure 4.27. *Principle diagram of the adaptation mechanism*

This method was developed by Schauder [SCH 92] under the name of MRAS (model reference adaptive system). For the estimation of the induction machine speed, he proposes a comparison of fluxes calculated, respectively, from stator and rotor equations. The basic idea is to find the speed parameter of the adaptable model providing two identical estimations of the flux. We can show that this value can only

be the true speed because there is uniqueness in the solution. The correct operation of this system is ensured by the judicious choice of a function $F_{\omega}(Y_{\mathrm{r}}, Y_{\mathrm{a}})$, ensuring convergence of the adaptable model toward the reference model, per the Popov criterion. The principle diagram is illustrated in Figure 4.27.

The drawback to the Schauder solution is that it bases the estimation of speed on distinct observers corresponding to stator or rotor equations that are of reduced order. We propose instead the Yang approach, where real current measures are the output of the reference model, which is actually the real machine. The output of the adaptable model is made up of stator currents estimated by the electrical variable observer. We calculate speed in such a way that the error between true and estimated currents cancels out. State models of the machine and observer are:

$$\begin{aligned} \dot{X} &= A(\omega)\cdot X + B\cdot U \quad \text{and} \quad Y = C\cdot X \\ \dot{X}^{*} &= A(\omega^{*})\cdot X^{*} + B\cdot U + K\left(\omega^{*}\right)\cdot C\left(X^{*} - X\right) \end{aligned} \qquad [4.58]$$

We consider the three basic matrices:

$$0 = \begin{bmatrix} 0 & 0 \\ 0 & 0 \end{bmatrix} \quad I = \begin{bmatrix} 1 & 0 \\ 0 & 1 \end{bmatrix} \quad J = \begin{bmatrix} 0 & -1 \\ 1 & 0 \end{bmatrix}$$

hence, state matrices:

$$A = \begin{bmatrix} a_1 I & a_2\left(a_4 I + \omega J\right) \\ a_3 I & a_4 I + \omega J \end{bmatrix} \quad B = \begin{bmatrix} bI \\ 0 \end{bmatrix} \quad C = \begin{bmatrix} I & 0 \end{bmatrix}$$

$$K\left(\omega^{*}\right) = \begin{bmatrix} k_1\left(\omega^{*}\right) I + k_2\left(\omega^{*}\right) J \\ k_3\left(\omega^{*}\right) I + \dfrac{k_2}{a_2}\left(\omega^{*}\right) J \end{bmatrix} \qquad [4.59]$$

$$a_1 = -\frac{1}{\sigma T_{\mathrm{s}}} - \frac{1-\sigma}{\sigma T_{\mathrm{r}}} \quad a_2 = -\frac{1-\sigma}{\sigma M_{\mathrm{sr}}} \quad a_3 = \frac{M_{\mathrm{sr}}}{T_{\mathrm{r}}} \quad a_4 = \frac{1}{T_{\mathrm{r}}} \quad b = \frac{1}{\sigma L_{\mathrm{s}}}$$

The state vector error: $e = X - X^{*}$ obeys a state equation:

$$\frac{\mathrm{d}e}{\mathrm{d}t} = A_{\mathrm{e}}(\omega)\cdot e - B_{\mathrm{e}}\cdot W(\varepsilon, X^{*}, t) \quad \text{with} \quad \varepsilon = C_{\mathrm{e}}\cdot e \qquad [4.60]$$

with:

$$e = \left[e(i_{s\alpha}) \quad e\left(i_{s\beta}\right) \quad e\left(\Phi_{r\alpha}\right) \quad e\left(\Phi_{r\beta}\right) \right]^t$$

$$A_e(\omega) = A(\omega) + K(\omega) \cdot C; \quad B_e = \begin{bmatrix} 1 & 0 & \frac{1}{a_2} & 0 \\ 0 & 1 & 0 & \frac{1}{a_2} \end{bmatrix}$$

ε represents estimation errors that can actually be calculated, that is, machine current errors. The above equation is illustrated in Figure 4.28.

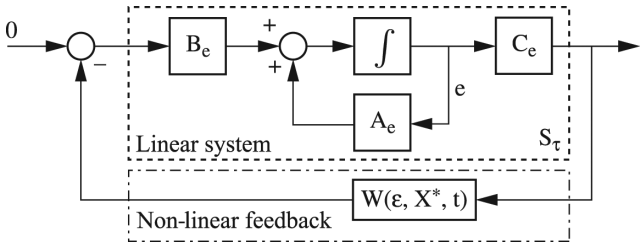

Figure 4.28. *Representation diagram of state equations of estimation errors*

The equivalent system is made up of a direct linear chain $S\tau$ and a non-linear feedback $W(\varepsilon, X^*, t)$. We have:

$$W = \left(\omega - \omega^*\right)\left(a_2 \begin{bmatrix} -\Phi^*_{r\beta} \\ \Phi^*_{r\alpha} \end{bmatrix} + k_2 \begin{bmatrix} -e\left(i_{s\beta}\right) \\ e\left(i_{s\alpha}\right) \end{bmatrix} \right) \qquad [4.61]$$

The observer convergence is equivalent to the asymptotic stability of the previous system. The determination of the three gains k_1, k_2, and k_3 and the law defining ω^* must make the system asymptotically stable. In order to do this, we use the hyperstability criterion from Popov [POP 73]:

1. the linear system $S\tau$ must be observable and controllable;

2. there is a symmetrical matrix P, defined positive, and a matrix Q, defined negative, such that:

$$A_e^t \cdot P + P \cdot A_e = Q \quad \text{and} \quad B_e^t \cdot P = C_e$$

3. there is a number γ_0 such that:

$$\int_0^t \varepsilon^t \cdot W \cdot \mathrm{d}\tau \geq -\gamma_0^2 \qquad [4.62]$$

The speed estimation law, cut off from previous considerations, was chosen in the form:

$$\Delta = \Phi_{r\beta}^* \left(i_{s\alpha} - i_{s\alpha}^* \right) - \Phi_{r\alpha}^* \left(i_{s\beta} - i_{s\beta}^* \right) \qquad [4.63]$$

where Δ represents the product of the estimation error of the electromagnetic torque, if the flux is correctly estimated. A non-zero value of Δ is interpreted as a speed estimation error. Function $F_\omega(\Delta)$, which provides the estimated speed, is the sum of a proportional part and an integral part of Δ, or in other words:

$$W = \omega^* = F_\omega(\Delta) = K_p \cdot \Delta + K_i \int_0^t \Delta \mathrm{d}\tau \qquad [4.64]$$

The advantages of this method are the following:

1. minimization of current estimation error;

2. no requirement to know the mechanical parameters of the machine;

3. low calculation volume.

The drawbacks are the following:

1. because of current measuring noises, the estimated speed is very noisy. This imposes the necessity of slowing down current and speed regulators to only amplify noises;

2. speed filtering before its consideration in the electrical Kalman filter leads to a delay that can put in question the adaptive method principle. This can lead to high amplitude fluctuations during transitory modes;

3. static speed error is directly linked to the numeric resolution prediction precision of the state of the electrical Kalman filter.

The choices of gains K_p and K_i are made with the help of consecutive simulations. To avoid large variations in the estimated speed, we limit the integral term, and the value of the limit is defined according to the electromagnetic torque. This

limit δT_{i} is defined with the help of a speed gap $\Delta\omega$ corresponding to the speed variation during a sampling period T_{s} during acceleration with the nominal torque:

$$\Delta\omega\left(T_{\mathrm{s}}\right)=\Gamma_{\mathrm{nom}}\cdot T_{\mathrm{s}}=\frac{\left(T_{\mathrm{em}}\right)_{\mathrm{nom}}\cdot T_{\mathrm{s}}}{J} \qquad [4.65]$$

We use an algorithm, which considers two types of operations:

1. low speed variation for an acceleration lower than 5% of T_{em};

2. high speed variation for an acceleration higher than 5% of T_{em};

Several simulations made it possible to define the algorithm according to these two operations.

$$Si\ \omega_{\mathrm{ref}}\left(n\right)-\omega_{\mathrm{ref}}\left(n-1\right)<0.05\Delta\omega\left(T_{\mathrm{e}}\right)$$
$$\delta T_{\mathrm{i}+}=0.5\Delta\omega\left(T_{\mathrm{e}}\right)$$
$$\delta T_{\mathrm{i}-}=-0.5\Delta\omega\left(T_{\mathrm{e}}\right)$$

$$Si\ \omega_{\mathrm{ref}}\left(n\right)-\omega_{\mathrm{ref}}\left(n-1\right)>0.05\Delta\omega\left(T_{\mathrm{s}}\right)$$
$$\delta T_{\mathrm{i}+}=\left[\omega_{\mathrm{ref}}\left(n\right)-\omega_{\mathrm{ref}}\left(n-1\right)\right]+2\Delta\omega\left(T_{\mathrm{s}}\right)$$
$$\delta T_{\mathrm{i}-}=\left[\omega_{\mathrm{ref}}\left(n\right)-\omega_{\mathrm{ref}}\left(n-1\right)\right]-2\Delta\omega\left(T_{\mathrm{s}}\right)$$

The principle diagram of this speed estimation adaptive system is given in Figure 4.29.

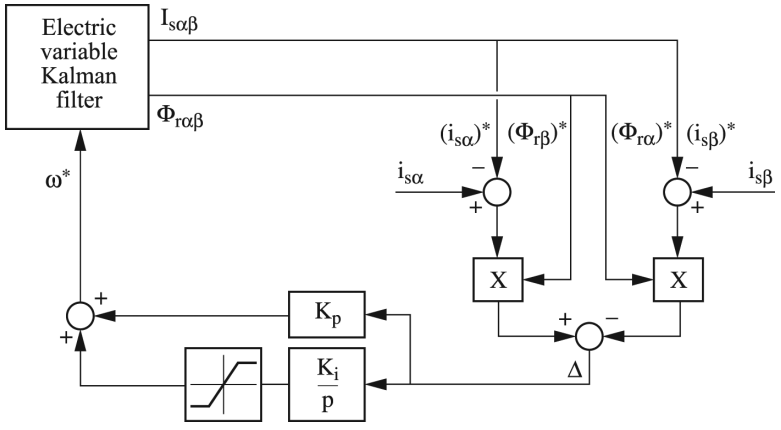

Figure 4.29. *Principle diagram of the speed estimation adaptive system*

Simulation tests illustrate (Figure 4.30) the behavior of the system. We can observe that the estimated speed and variable V_{sq} are very noisy (Figure 4.30, curve 1).

Improvements are made by the reduction of noises, according to the algorithm above involving the limitation of the integral term (Figure 4.30, curve 2). Filtering and the reduction of regulator dynamic (Figures 4.30, curves 3 and 4) bring significant improvement.

4.6.3.4. *Adaptive mechanism associated with a mechanical observer*

As we have seen in section 4.6.3.2, the mechanical observer enables speed filtering and load torque estimation. The use of MRAS provides an estimation of the speed by going beyond the calculation of the sliding frequency that greatly depends on rotor resistance. For systems with a long sampling period, it is the inaccuracy of the numeric resolution in the prediction phase of the electrical Kalman filter.

We use the same function Δ than in the previous section, and the state equation of the mechanical observer contains terms proportional to Δ:

$$\frac{\mathrm{d}}{\mathrm{d}t}\begin{bmatrix}\omega^* \\ C_\mathrm{r}^*\end{bmatrix} = \begin{bmatrix}-\frac{f}{J} & -\frac{P}{J} \\ 0 & 0\end{bmatrix}\begin{bmatrix}\omega^* \\ C_\mathrm{r}^*\end{bmatrix} + \begin{bmatrix}\frac{P}{J} \\ 0\end{bmatrix} T_\mathrm{em} + \begin{bmatrix}k_\omega \\ k_\mathrm{Cr}\end{bmatrix}\Delta \qquad [4.66]$$

The prediction of states is done from the mechanical equation and correction of term Δ, resulting from current measures. k_Tl defines the quality and speed of estimation of the load torque, and k_ω the stability and quality of estimated speed filtering.

The principle diagram of the MRAS and mechanical Kalman filter association are shown in Figure 4.31.

The speed estimation law is given by the integral–differential equation deduced from the previous state equation:

$$\frac{\mathrm{d}\omega^*}{\mathrm{d}t} = -\frac{1}{\tau_\mathrm{m}}\omega^* + \frac{P}{J}T_\mathrm{em} + k_\omega\Delta - k_\mathrm{Tl}\frac{P}{J}\int_0^\mathrm{t}\Delta\left(\varepsilon, X^*, \tau\right)\mathrm{d}\tau \qquad [4.67]$$

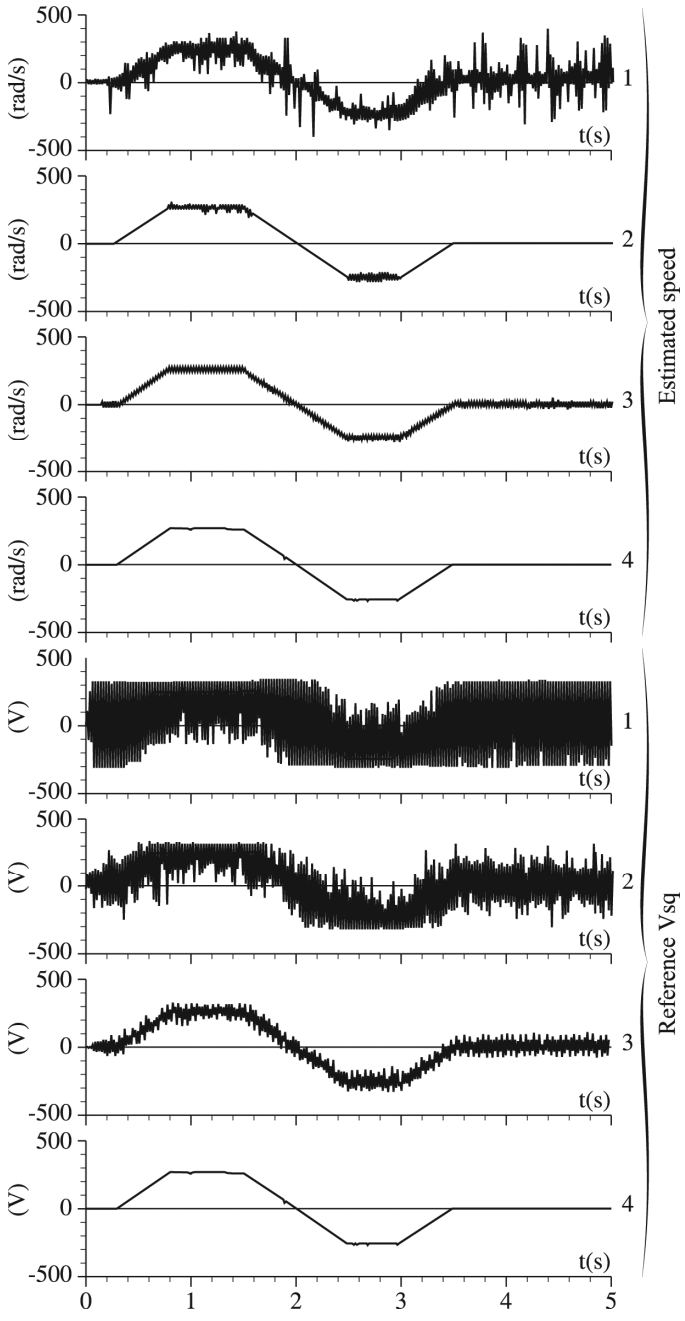

Figure 4.30. *Simulation results with adaptive estimation*

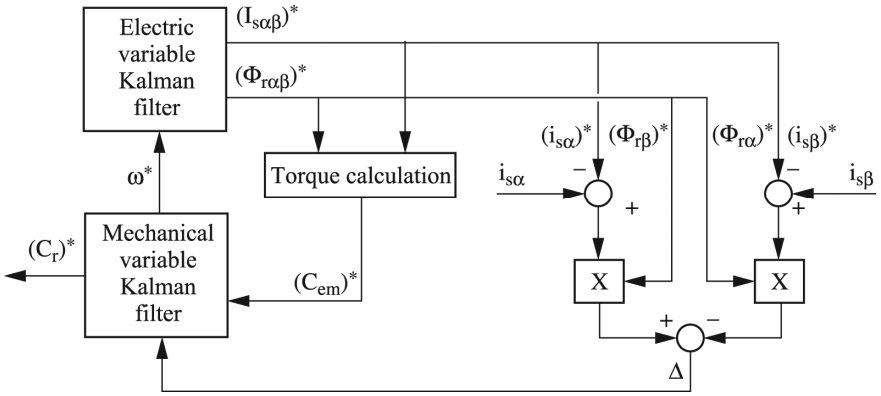

Figure 4.31. *Principle diagram of the association between the adaptive mechanism and the mechanical Kalman filter for the estimation of speed*

and the solution is:

$$\omega^* = G\int_0^t \Delta\left(\varepsilon, X^*, \tau\right)\mathrm{d}\tau + G(a-1)V(t)$$
$$V(t) = e^{-(t/\tau_\mathrm{m})}\int_0^t e^{-(t/\tau_\mathrm{m})}\cdot\Delta\left(\varepsilon, X^*, \tau\right)\cdot\mathrm{d}\tau \qquad [4.68]$$

where $G = \dfrac{P\cdot K_{\mathrm{Tl}}}{f}$ and $a = \dfrac{f\cdot k_\omega}{P\cdot K_{\mathrm{Tl}}}$

The last step consists of choosing G and a in order to satisfy the Popov criterion, maintaining adequate decoupling between the flux and torque, and having low noise levels on the signals. The transfer function between the estimated speed and quantity Δ is given by:

$$\frac{\omega^*}{\Delta} = G\frac{(1+a\cdot\tau_\mathrm{m}\cdot p)}{p(1+\tau_\mathrm{m}\cdot p)} \qquad [4.69]$$

If $a<1$, we have a phase delay, and filtering is more efficient.

If $a>1$, we have an advance in phase, and looped system stability is better.

K_{Tl} is used to set the transfer function gain above, and k_ω is used to define a.

For the speed and torque profile defined previously (Figure 4.26 and section 4.6.3.2), we present two series of results:

1. Figure 4.32 in which a is set and G has three different values;

2. Figure 4.33 in which G is set and a takes three different values.

For the machine considered, the best compromise between speed of response and minimization of noises corresponds to values: $a = 0.0036$ and $G = 11.1$.

4.7. Adaptive observer

4.7.1. *Introduction*

The structure of observation that we are now developing is a specific rotor flux observer. In fact, it must rebuild the two components of the rotor flux and estimate the speed at the same time. It is based on the MRAS technique, presented in section 4.6.3.3 only for the estimation of speed and is applicable to the observation of the flux. This method consists of adapting the operation of an adjustable system to that of a reference model (Figure 4.34). The adaptation organ modifies the parameters of the adjustable system (observer) to obtain rotor flux Φ_r^* and speed ω^* by decreasing the estimation error of stator currents.

To create this observer, we can proceed in two ways. The first one uses an appropriate *Lyapunov function*, and its research is quite complicated. The second method, retained for our study, is based on *the hyperstability theory of Popov* (4.6.3.3 and [4.62]). The system is described by a state equation in stationary reference frame (α_s, β_s) where the dynamic matrix depends on speed ω^* ([4.58] and [4.59]).

$$A\left(\omega^*\right)=\begin{bmatrix} a_1 & 0 & a_2a_4 & -a_2\omega^* \\ 0 & a_1 & a_2\omega^* & a_2a_4 \\ a_3 & 0 & a_4 & -\omega^* \\ 0 & a_3 & \omega^* & a_4 \end{bmatrix},\quad B=\begin{bmatrix} b & 0 & 0 & 0 \\ 0 & b & 0 & 0 \end{bmatrix}^{\mathrm{T}},\quad C=\begin{bmatrix} 1 & 0 & 0 & 0 \\ 0 & 1 & 0 & 0 \end{bmatrix} \qquad [4.70]$$

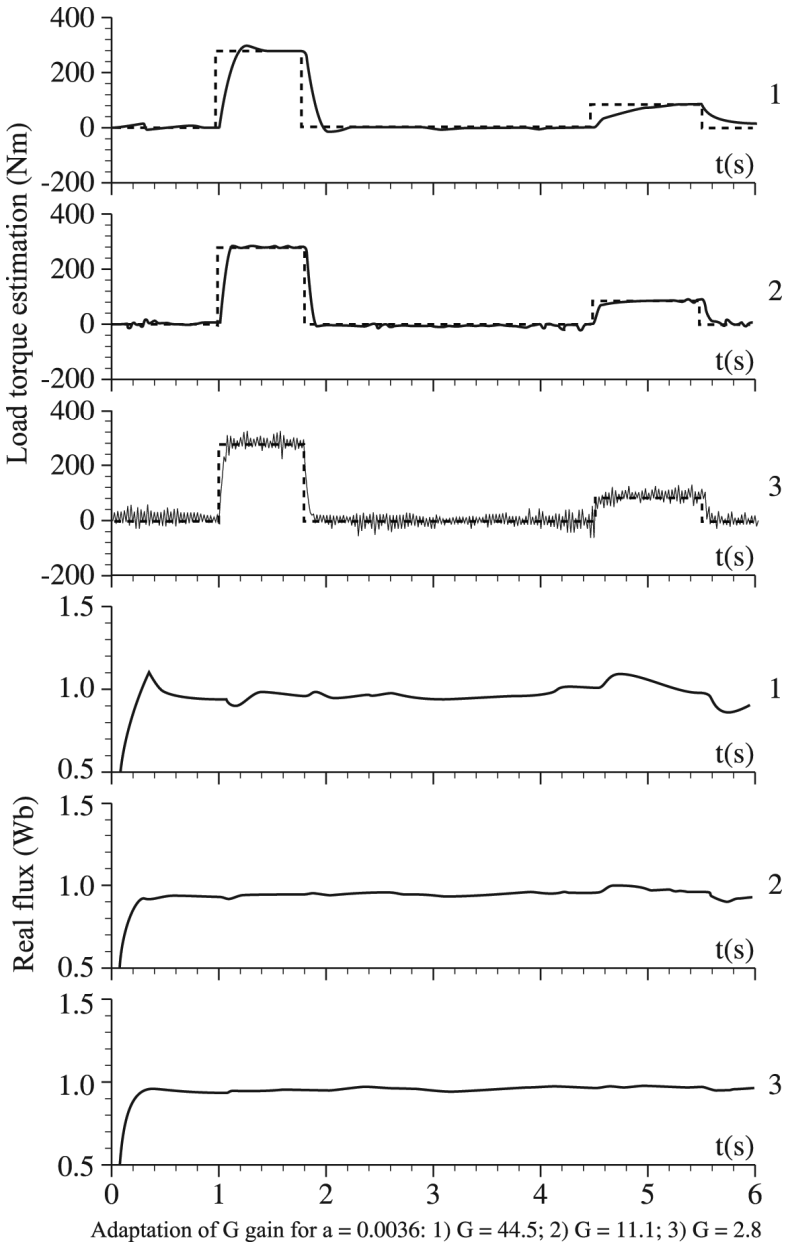

Figure 4.32. *Estimation of load torque for a constant and G variable*

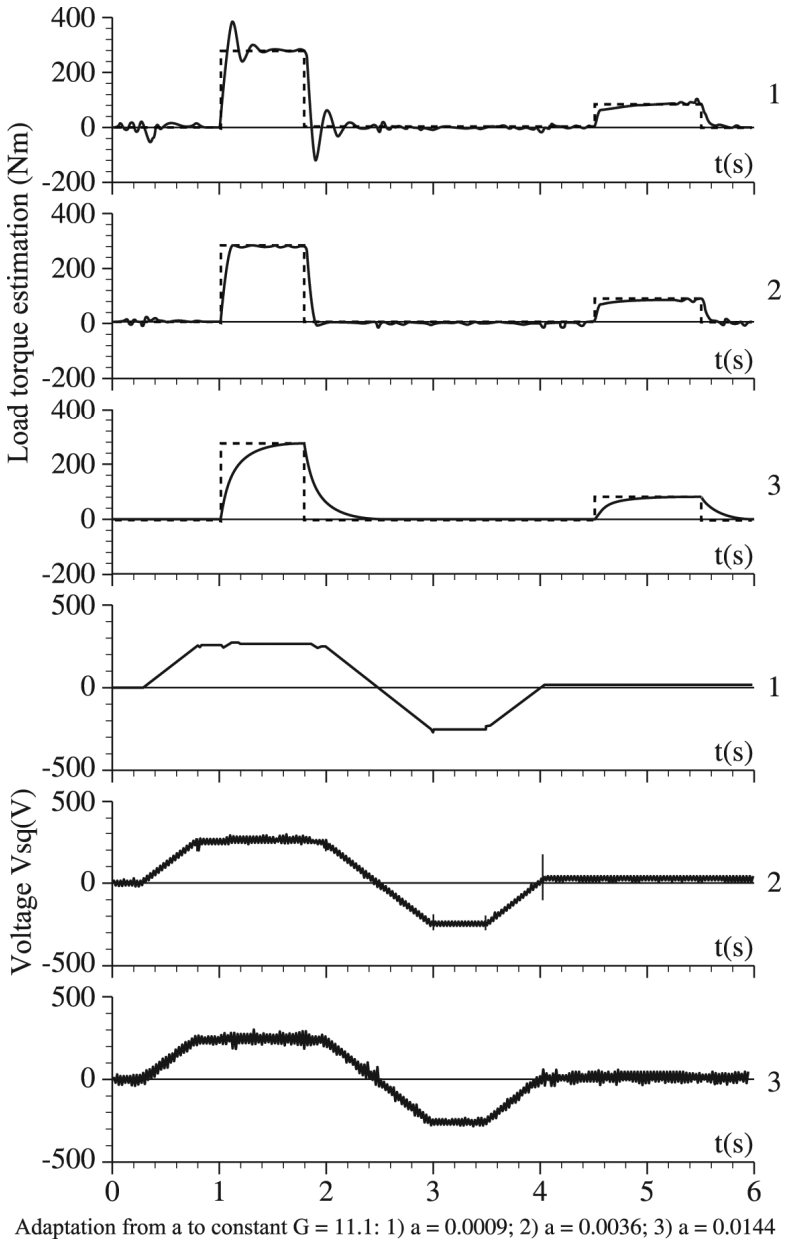

Figure 4.33. *Estimation of load torque with G constant and a variable*

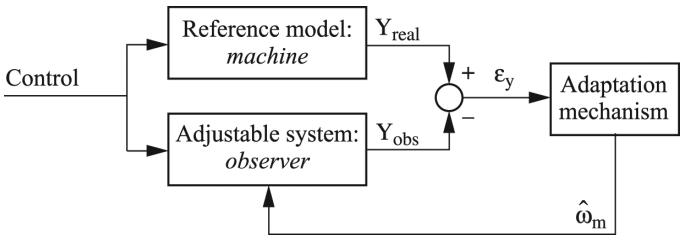

Figure 4.34. *Principle of an adaptive system*

Matrix $A\left(\omega^*\right)$ is antisymmetrical, and we will keep this characteristic for the creation of the observer. Gain matrix $K\left(\omega^*\right)$ will have a structure that is written as:

$$K\left(\omega^*\right)=\begin{bmatrix} k_1 & -k_2\omega^* \\ k_2\omega^* & k_1 \\ k_3 & -(k_2/a_2)\omega^* \\ (k_2/a_2)\omega^* & k_3 \end{bmatrix} \qquad [4.71]$$

If a system is made up of a linear invariant Σ_L part in the direct chain and a non-linear part W in the feedback chain (Figure 4.35), then it is said to be asymptotically stable if the hyperstability of Popov conditions are verified (section 4.6.3.3 and [4.62]).

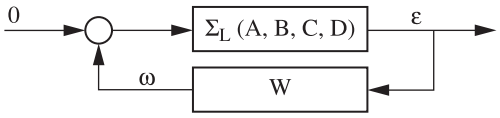

Figure 4.35. *Breakdown of the linear Σ_L part and non-linear W part system*

The state equations of the estimation error and non-linear function W are given in section 4.6.3.3. The block diagram is represented in Figure 4.28.

According to Popov, the asymptotic stability of this system is equivalent to observer convergence. But this theorem only guarantees the convergence of state estimation (e = 0) and not that of the speed. However, convergence of e toward zero involves that of ω^* toward ω since the equation of the error is

$$\dot{e} = A_e \cdot e - \left(A(\omega) - A\left(\omega^*\right)\right) \cdot X^* - \left(K(\omega) - K\left(\omega^*\right)\right) \cdot C \cdot e \qquad [4.72]$$

If the convergence of the observer is ensured, we get

$$\left(A(\omega)-A\left(\omega^*\right)\right)\cdot X^* = 0 \Rightarrow \left(\omega-\omega^*\right)\cdot\begin{bmatrix}-\Phi_{r\beta}\\ \Phi_{r\alpha}\end{bmatrix} = 0 \qquad [4.73]$$

For $\Phi_{r\alpha} \neq 0$ or $\Phi_{r\beta} \neq 0$, we deduce that true speed ω is equal to estimated speed ω^*.

4.7.2. *Determination of observer gains*

We must define observer gains respecting the conditions of the Popov theory. Matrix *P*, not involved in the development of the observer, is used to prove the stability of the system, and it is chosen in order to make calculations easier. For example:

$$P=\begin{pmatrix} x_1 I & x_3 I - x_4 J \\ x_3 I - x_4 J & x_2 I \end{pmatrix} \quad \text{where} \quad I=\begin{pmatrix}1 & 0\\ 0 & 1\end{pmatrix} \quad \text{and} \quad J=\begin{pmatrix}0 & 1\\ -1 & 0\end{pmatrix} \qquad [4.74]$$

Matrix *Q* becomes

$$Q=\begin{pmatrix} a\cdot I & b\cdot I + c\cdot\omega\cdot J \\ b\cdot I - c\cdot\omega\cdot J & d\cdot I \end{pmatrix} \qquad [4.75]$$

with

$$\begin{cases} a = 2\left(a_1+k_1\right)\cdot x_1 + 2\left(a_3+k_3\right)\cdot x_3 + 2\dfrac{k_2}{a_2}\cdot\omega\cdot x_4 \\ b = \left(a_1+k_1+a_4\right)\cdot x_3 + \left(\left(1-k_2\right)\omega\right)\cdot x_4 + a_2\cdot a_4\cdot x_1 + \left(a_3+k_3\right)\cdot x_2 \\ c\cdot\omega = a_2\cdot\omega\cdot x_1 + \omega\left(1-k_2\right)\cdot x_3 - \left(a_1+k_1+a_4\right)\cdot x_4 - \dfrac{k_2}{a_2}\cdot\omega\cdot x_2 \\ d = 2a_2\cdot a_4\cdot x_3 - 2a_2\cdot\omega\cdot x_4 + 2a_4\cdot x_2 \end{cases}$$

We then demonstrate that *Q* is defined negative and *P* positive. For this, we turn *Q* into a diagonal form by canceling *b* and *c* factors:

$$b = 0:\ k_2 = 1 = x_1, \quad x_4 = 0, \quad \text{and} \quad x_2 = a_2^2$$

$$c = 0:\ x_3 = \frac{-a_2\left(a_4 + a_2\cdot\alpha_3\right)}{\left(a_4+\alpha_1\right)} \qquad [4.76]$$

we write:

$$\alpha_1 = a_1 + k_1 \text{ and } \alpha_3 = a_3 + k_3$$

Q will be defined as negative if its diagonal elements are strictly negative. By noting:

$$\beta = \frac{-a_2\left(a_4 + a_2 \cdot \alpha_3\right)}{\left(a_4 + \alpha_1\right)}$$

Q and P become:

$$Q = \begin{pmatrix} 2\left(\alpha_1 + \alpha_3 \cdot \beta\right) \cdot I & 0 \\ 0 & 2a_2 \cdot a_4\left(a_2 + \beta\right) \cdot I \end{pmatrix} \qquad P = \begin{pmatrix} I & \beta \cdot I \\ \beta \cdot I & a_2^2 \cdot I \end{pmatrix} \quad [4.77]$$

P will be defined as positive if all its main minors are strictly positive:

$$|a_2| > |\beta| \Rightarrow -2a_4 - \alpha_1 > a_2 \cdot \alpha_3 > \alpha_1 \quad [4.78]$$

Q will be defined as negative if:

$$\alpha_1 + \alpha_3 \cdot \beta < 0 \quad [4.79]$$

The association of these disparities [4.78] and [4.79] gives the condition for k_3, definitely fixed when k_1, which is involved in the adaptation of the law of ω, is defined. Then:

$$\alpha_1 < a_2 \cdot \alpha_3 < 0 \Rightarrow -a_3 < k_3 < \frac{\left(\alpha_1 - a_2 \cdot a_3\right)}{a_2} \quad [4.80]$$

P is fixed, and C_e [4.62] is defined by the Popov theorem.

4.7.3. *Speed adaptation law*

4.7.3.1. *Verification of the third condition of the hyperstability theory*

The ω^* adaptation law will be determined by using the third condition of Popov [4.62], which comes down to finding a lower bound of the function:

$$f(t) = \int_0^t \varepsilon^T \cdot W \cdot \mathrm{d}t \quad [4.81]$$

or:

$$f(t) = \int_0^t F \cdot S(t) \cdot \mathrm{d}t \qquad [4.82]$$

$$\begin{cases} \varepsilon^{\mathrm{T}} = C_{\mathrm{e}} \cdot e = \left((\alpha_1 - a_2 \cdot \alpha_3 / a_4 + \alpha_1) \right) \cdot \left[I \quad a_2 \cdot I \right] \cdot e \\ S(t) = y^{\mathrm{T}} \cdot \left(a_2 \cdot \begin{bmatrix} -\Phi_{\mathrm{r}\beta} \\ \Phi_{\mathrm{r}\alpha} \end{bmatrix} + \begin{bmatrix} -e_{\mathrm{is}\beta} \\ e_{\mathrm{is}\alpha} \end{bmatrix} \right) \\ F = \omega - \omega^* \end{cases} \qquad [4.83]$$

We choose adaptation law:

$$\omega^* = -L \cdot \int_0^t S(t) \mathrm{d}t \qquad [4.84]$$

where L is the coefficient giving speed estimation. The dynamic of ω^* is set 10 times faster than that of ω, for it to catch up. Consequently, we ignore the variations of ω, in relation to those of ω^*:

$$\dot{F} = \dot{\omega} - \dot{\omega}^* = -\dot{\omega}^* = -L \cdot S(t) \Rightarrow f(t) = \frac{1}{L} \int_0^t F \cdot \dot{F} \cdot \mathrm{d}t = \frac{1}{2L} \left(F^2(t) - F^2(0) \right) \qquad [4.85]$$

$$\text{If} : f(t) \geq -\frac{1}{2L} F^2(0) \qquad \forall t \ .$$

4.7.3.2. *Parameters* k_1 *and* L_1

We have already verified the three conditions of the Popov hyperstability theory. We now define the characteristics of the law of adaptation that are fixed for values of L and k_1. By developing this law, we obtain [4.86]:

$$\omega^* = -La_2 \frac{\alpha_1 - a_2 \alpha_3}{a_4 + \alpha_1} \int_0^t \left[T_1 + T_2 + T_3 \right] \mathrm{d}t \qquad [4.86]$$

where [4.87]:

$$T_1 = e_{\mathrm{is}\beta} \hat{\Phi}_{\mathrm{r}\alpha} - e_{\mathrm{is}\alpha} \hat{\Phi}_{\mathrm{r}\beta}, \quad T_2 = e_{\Phi \mathrm{r}\varphi} \hat{\Phi}_{\mathrm{r}\alpha} - e_{\Phi \mathrm{r}\alpha} \hat{\Phi}_{\mathrm{r}\beta}, \quad \text{and} \quad T_3 = e_{\Phi \mathrm{r}\beta} e_{\mathrm{is}\alpha} - e_{\Phi \mathrm{r}\alpha} e_{\mathrm{is}\beta}$$

The third term T_3 of the integrant can be ignored in relation to the first T_1, since the flux error is low in relation to the value of the reference flux (order two error is

ignored in relation to order one error). θ_r being the angle between the direction of the real flux and estimated flux; the second term becomes:

$$a_2 \int_0^t \left(\left| \Phi_r \right| \cdot \sin\left(\theta_r\right) \cdot \mathrm{d}t \right) \qquad [4.87]$$

If the observer converges, the flux is stabilized in sinusoidal mode, $\theta_r = 0$, making it possible to ignore this term. The law of adaptation is reduced to:

$$\omega^* = L_1 \cdot \int_0^t \left(e_{is\beta} \cdot \hat{\Phi}_{r\alpha} - e_{is\alpha} \cdot \hat{\Phi}_{r\beta} \right) \mathrm{d}t \quad \text{with} \quad L_1 = -L \cdot a_2 \frac{\alpha_1 - a_2\alpha_3}{a_4 + \alpha_1} \qquad [4.88]$$

To determine L_1, we study the estimated speed dynamic from the previous equation and the speed estimation error equation:

$$e_\omega = \omega^* - \omega \qquad [4.89]$$

The result then is:

$$\begin{aligned} \dot{\dot{e}}_\omega - \left(a_4 + \alpha_1\right)\dot{e}_\omega + L_1 a_2 e_\omega & \left(\begin{array}{l} \left(1/a_2^2\right)\left(e_{is\alpha}{}^2 + e_{is\beta}^2\right) - \\ \left(\Phi_{r\alpha}^2 + \Phi_{r\beta}^2\right) - \left(\hat{\Phi}_{r\alpha} e_{\Phi r\alpha} + \hat{\Phi}_{r\beta} e_{\Phi r\beta}\right) \end{array} \right) = \\ & - \left(L_1/a_2\right)\omega\left(e_{is\alpha}{}^2 + e_{is\beta}^2\right) + L_1 a_2 \omega\left(\hat{\Phi}_{r\alpha} e_{\Phi r\alpha} + \hat{\Phi}_{r\beta} e_{\Phi r\beta}\right) \\ & - L_1 a_2 a_4 \left(\hat{\Phi}_{r\beta} e_{\Phi r\alpha} - \hat{\Phi}_{r\alpha} e_{\Phi r\beta}\right) \end{aligned} \qquad [4.90]$$

Since these electric variables are much faster than speed, the errors of the four electric variables quickly cancel out in relation to that of the speed. The previous equation can be approximated by

$$\dot{\dot{e}}_\omega - \left(a_4 + \alpha_1\right) \cdot \dot{e}_\omega - L_1 \cdot a_2 \cdot e_\omega \cdot \left| \hat{\Phi}_r \right|^2 = 0 \qquad [4.91]$$

with: $\alpha_1 = a_1 + k_1$.

In order for the speed estimation error to cancel out, coefficient $\left(a_4 + \alpha_1\right)$ must be negative. The differential equation obtained is of the second order, defined by

$$2\xi\omega_n = -\left(a_4 + \alpha_1\right) \quad \text{and} \quad \omega_n^2 = -L_1 \cdot a_2 \cdot \left| \Phi_r^* \right|^2$$

The choice of L_1 is done in such a way that ω^* is at least 10 times faster than the closed loop speed. If T_m is the undampened period of speed ω and T_e is that of ω^*: $T_e = 2\pi/\omega_{n_{\hat{w}}} = T_m/10$.

Then gain L_1 becomes:

$$L_1 = \frac{(2\pi 10)^2}{-a_2 \left|\Phi_r^*\right|^2 T_m^2} \qquad [4.92]$$

k_1 sets dampening of e_w according to the expression:

$$\xi = \frac{(a_4 + a_1 + k_1)T_m}{40\pi} \qquad [4.93]$$

L_1 and k_1 are therefore defined by the conditions imposing the desired convergence of the estimation error. Once k_1 is set, we determine k_3 by relation [4.80] and all observer gains are defined.

4.7.4. Simulation results and experimental results

We tested the operation of the variable speed drive with the complete control implemented according to scenario [AND 96].

1. Establishment of nominal flux, $|\Phi_r| = 0.2613$ Wb, at $t = 0$ s.

2. Startup of the variable speed drive to its rated electric speed 270 rad/s at $t = 0.2$ s.

3. Imposition of a constant load torque, $C_0 = 1$ Nm, at $t = 0.5$ s.

4. Reversal rotation direction at $t = 0.8$ s and maintenance of the generator operation from $t = 1.6$ s to $t = 2$ s.

5. Reset of the speed at -3 rad/s to $t = 2$ s.

We can observe (Figure 4.36a) that the rotor flux is quickly installed, its observation is satisfactory, and it quickly converges at real value. Speed is also controlled in a very satisfactory manner ($T_s = T_{dec} = 250.10^{-6}$ s). We must note that

speed and flux behaviors are satisfactory at every point in the variable speed drive operation and even at very low speed.

In this case, we have complementary information on the torque and load torque (Figure 4.36b) that can be used for a possible compensation.

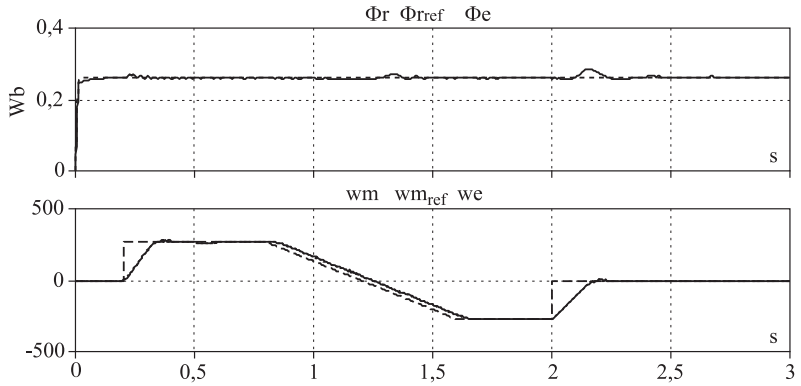

Figure 4.36a. *Responses of rotor flux and rotation speed, the straight line represents Φ_r and Φ_e (estimated flux) taken together or ω_m and ω_e (estimated speed) and the dotted line corresponds to flux and speed references, respectively*

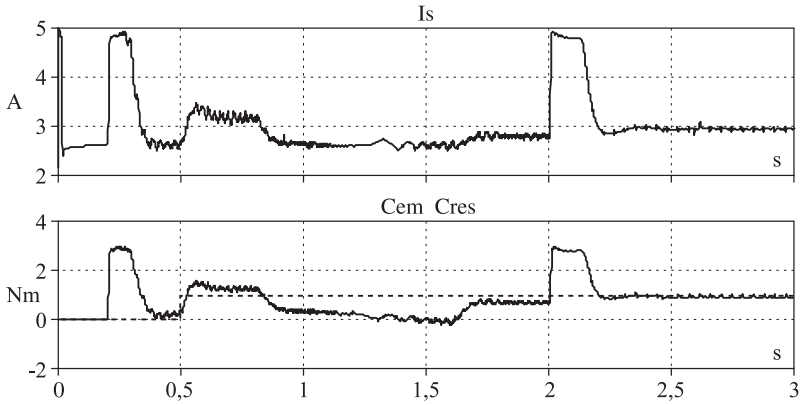

Figure 4.36b. *Responses of stator current, electromagnetic torque, and load torque. T_{em} is the straight line gradient and C_{res} the dotted line*

In order to have correct operation of the low-speed variable speed drive with constant load torque, we have injected the 200-Hz sinusoidal signal in the flux axis. This is done to enrich the harmonic content of the voltage that will enable the correct estimation of the speed at the point of operation where ω_s goes through zero. Figure 4.37 shows that the flux perfectly follows its reference when there is injection of the high-frequency signal, which is not the case when there is no injection. In this last case, speed and flux diverge.

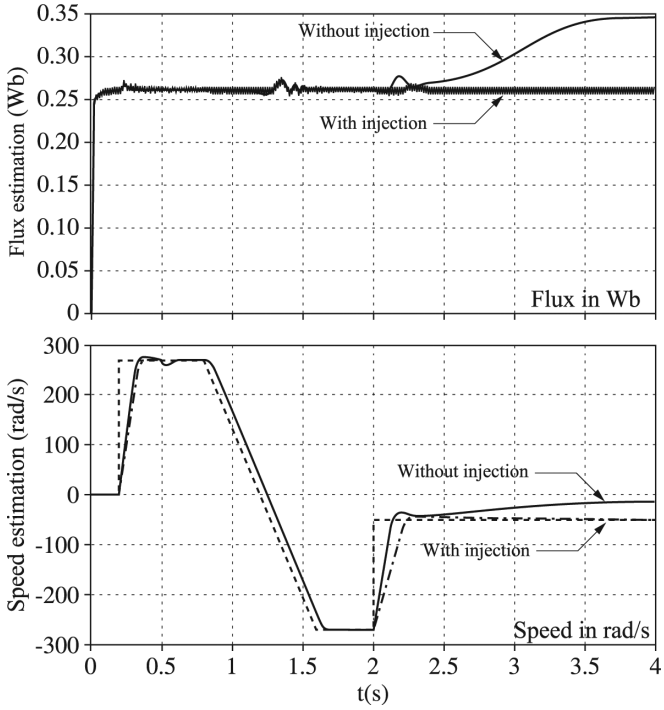

Figure 4.37. *Estimation of speed at low speed with injection of 200-Hz sinusoidal signal in the flux axis*

Figure 4.38 shows the behavior of the variables that interest us. The flux very quickly responds and stays at a constant value during the transitory mode.

The mechanical speed responds in 200 ms, with an over shoot of 2% as a Butterworth filter. We can verify that the static error of the speed estimation is lowered by 2% in motor operation as well as in generator operation.

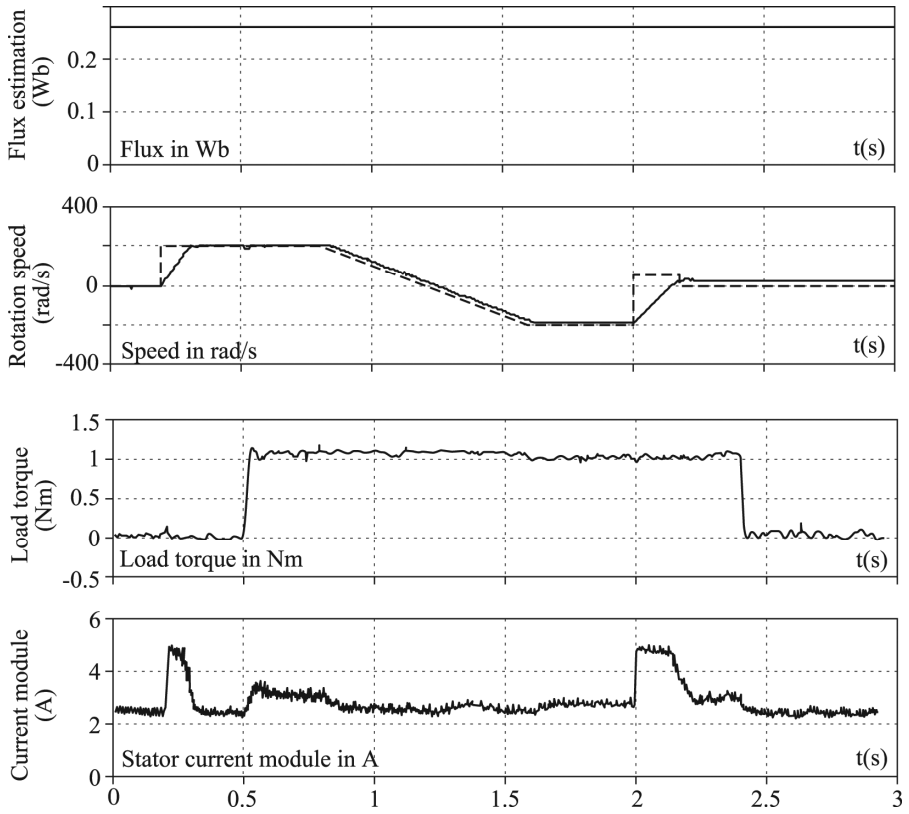

Figure 4.38. *Experimental results, response of rotor flux, rotation speed load torque, and stator current (image of the electromagnetic torque)*

Overspeed operation of the variable speed drive is shown in Figure 4.39. We can verify that the speed response time in the second transitory mode is almost the same as in the first. Therefore, response time is independent from the flux level.

4.8. Variable structure mechanical observer (VSMO)

4.8.1. *Basic principle*

The speed observer presented here is developed according to the sliding mode principle [ARC 99, BUH 86, UTK 81]. This type of observer is interesting because of its robustness in terms of uncertainties of modeling applied. The mathematical bases of variable structure observation or control are the theory of discontinuous second member differential equations developed by Fillipov.

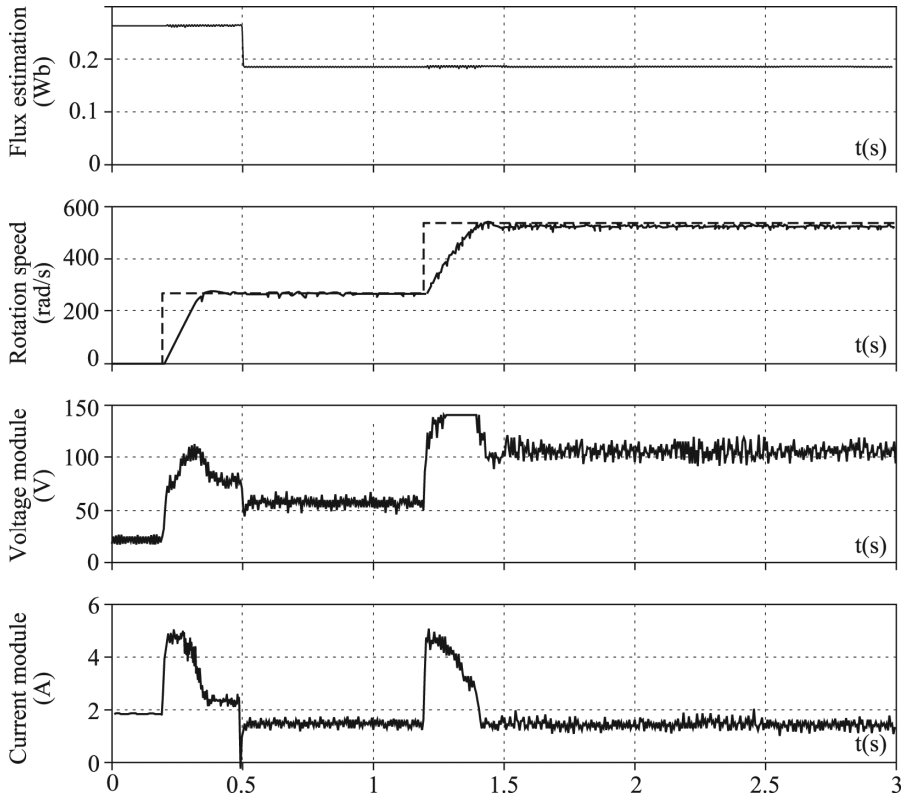

Figure 4.39. *Experimental results corresponding to overspeed operation. Responses of flux, rotation speed, stator voltage and stator current*

A system described by the following differential equation:

$$\frac{\mathrm{d}}{\mathrm{d}t}X = f\left(X,t\right) \qquad [4.94]$$

and $\hat{f}\left(X,t\right)$, an approximate function where inaccuracies are increased by a known continuous function:

$$\left\|\hat{f}\left(X,t\right) - f\left(X,t\right)\right\| < F\left(X,t\right) \qquad [4.95]$$

The observer must provide an observed value for the state of system $\hat{X}$ as close to its true value as possible. The S sliding surface is reached when the state observed equals the true state:

$$S = C \cdot \left(\hat{X} - X \right) = 0 \qquad [4.96]$$

We can then formulate the observer structure in the following way:

$$\frac{\mathrm{d}}{\mathrm{d}t} \hat{X} = \hat{f}\left(\hat{X}, t \right) + U_{\text{obs}} \qquad [4.97]$$

U_{obs} corresponds to control to correct observation errors, and we must choose it for the S sliding surface to be a stable balance surface of the observer. We use the stability method defined by Lyapunov in which the Lyapunov $V(S)$ function is written as

$$V\left(S \right) = \frac{1}{2} \cdot S^2 \qquad [4.98]$$

This function is defined as positive, that is,

$$V\left(0 \right) = 0 \quad \text{and if} \quad S \neq 0 \text{, then } V\left(S \right) > 0$$

In order for the S sliding surface to be attractive and stable, the first derivative of $V(S)$ must be a function defined as negative. Or

$$\frac{\mathrm{d}}{\mathrm{d}t} V\left(S \right) = S \cdot \frac{\mathrm{d}}{\mathrm{d}t} S = S \cdot \left[C \cdot \left(\hat{f} - f + U_{\text{obs}} \right) \right] < 0 \qquad [4.99]$$

We now choose a control such as $U_{\text{obs}} = -K.\text{sgn}\left(S \right)$ with $K > 0$. The variable structure observer has as structure:

$$\begin{cases} \dfrac{\mathrm{d}}{\mathrm{d}t} \hat{X} = \hat{f}\left(\hat{X}, t \right) - K \cdot \text{sgn}\left(S \right) \\ \quad \hat{Y} = C \cdot \hat{X} \end{cases} \qquad [4.100]$$

Because of the discontinuous function K·sgn (S), the n order observation system has to converge to an order ($n - m$) surface, where m is the number of measurable outputs of the system observed.

4.8.2. *Construction of the VSMO*

The action model of the system for the proposed observation uses the principle of electric and mechanical mode separation of the induction machine. In this way, the mechanical speed (its evolution is very slow compared to the evolution of electrical dimensions) can be considered as a parameter in electric equations.

The VSMO is in the following form:

$$\begin{cases} \dfrac{\mathrm{d}}{\mathrm{d}t}\hat{X}_{\mathrm{m}} = A_{\mathrm{m}} \cdot \hat{X}_{\mathrm{m}} + B_{\mathrm{m}} \cdot U_{\mathrm{m}} \\ \hat{Y}_{\mathrm{m}} = C_{\mathrm{m}} \cdot \hat{X}_{\mathrm{m}} \end{cases} \qquad [4.101]$$

with $\hat{X}_{\mathrm{m}} = \begin{pmatrix} \hat{\omega}_{\mathrm{m}} \\ \hat{C}_{\mathrm{r}} \end{pmatrix}$ state vector, $U_{\mathrm{m}} = C_{\mathrm{em}}$, and matrices A_{m}, B_{m} and C_{m} defined, respectively:

$$A_{\mathrm{m}} = \begin{pmatrix} -\dfrac{f_{\mathrm{m}}}{J_{\mathrm{m}}} & -\dfrac{P_{\mathrm{p}}}{J_{\mathrm{m}}} \\ 0 & 0 \end{pmatrix}, \quad B_{\mathrm{m}} = \begin{pmatrix} \dfrac{P_{\mathrm{p}}}{J_{\mathrm{m}}} \\ 0 \end{pmatrix}, \quad \text{and} \quad C_{\mathrm{m}} = \begin{pmatrix} 1 & 0 \end{pmatrix}$$

$$L = \begin{bmatrix} -l_1 \\ -l_2 \end{bmatrix} \quad \text{and} \quad K = \begin{bmatrix} -k_1 \\ -k_2 \end{bmatrix} \quad \text{and gain vectors of the observer.}$$

The sliding surface is chosen; it involves the components of the state vector that can be obtained by measure, or as in the case studied where the rotation speed is obtained by the composition of electric angular frequencies (previously discussed in section 4.6.3.1). We then obtain:

$$S = \hat{\omega}_{\mathrm{m}} - \omega_{\mathrm{mmes}} = \tilde{\omega}_{\mathrm{m}} \qquad [4.102]$$

The discontinuous function $K \cdot \mathrm{sgn}\left(\tilde{\omega}_{\mathrm{m}}\right)$ maintains the course of the state vector observed on the sliding surface. The term $\mathrm{L} \cdot \tilde{\omega}_{\mathrm{m}}$ widens the area of direct attraction of the sliding surface and enables better convergence of the variable observed toward the surface regardless of the initial conditions. However, this term is not necessary to the convergence of the observer. If vector K is zero, the observer then becomes a Luenberger deterministic observer where the determination of vector L gains can be obtained by a pole placement technique of the linearized system.

The global diagram of control with VSMO is illustrated in Figure 4.40 [ARC 99]. We deduct the estimated value from the mechanical speed by the selfpiloting relation. This value then plays the role of "measure" to converge the observer toward the sliding surface.

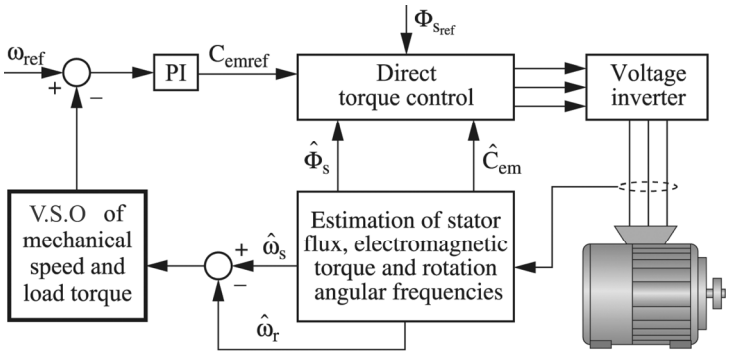

Figure 4.40. *Global diagram of control containing the variable structure observer*

4.8.3. *Determination of variable structure observer gains*

As was addressed in section 4.8.1, vector *K* gains are chosen in such a way that the sliding condition must be verified:

$$S \cdot \frac{\mathrm{d}}{\mathrm{d}t} S < 0 \qquad [4.103]$$

In order to do this, we must characterize the observation error and its evolution. We obtain the differential system [4.101] characterizing the observation error $\tilde{\omega}_{\mathrm{m}}$:

$$\begin{cases} \dfrac{\mathrm{d}}{\mathrm{d}t}\tilde{\omega}_{\mathrm{m}} = \dfrac{f_{\mathrm{m}}}{J_{\mathrm{m}}} \cdot \tilde{\omega}_{\mathrm{m}} - \dfrac{p_{\mathrm{n}}}{J_{\mathrm{m}}} \cdot T_{\mathrm{l}} - l_1 \cdot \tilde{\omega}_{\mathrm{m}} - k_1 \cdot \mathrm{sgn}\left(\tilde{\omega}_{\mathrm{m}}\right) \\ \dfrac{\mathrm{d}}{\mathrm{d}t} T_{\mathrm{l}} = -l_2 \cdot \tilde{\omega}_{\mathrm{m}} - k_2 \cdot \mathrm{sgn}\left(\tilde{\omega}_{\mathrm{m}}\right) \end{cases} \qquad [4.104]$$

By solving the sliding condition with the expression of $\dot{\tilde{\omega}}_{\mathrm{m}}$ and in the case of a system sampled at T_s, we obtain:

$$k_1 > \left(1-\lambda\right) \cdot \max \left| \left(\frac{f_{\mathrm{m}}}{J_{\mathrm{m}}} - l_1 \right) \cdot \tilde{\omega}_{\mathrm{m}} - \frac{P_{\mathrm{p}}}{J_{\mathrm{m}}} \cdot T_{\mathrm{e}} \right| \quad \text{or} \quad \lambda = \mathrm{e}\left(-\frac{\mathrm{f_m}}{\mathrm{J_m}} \times \mathrm{T_s} \right) \qquad [4.105]$$

The maxima reachable by the mechanical speed and load torque of the system studied helps in choosing gain k_1 so that it can verify the disparity [4.103]. On the sliding surface, the order two systems are degenerated into a first-order system and equations [4.106] are verified:

$$\begin{aligned} S = 0 &\Leftrightarrow \tilde{\omega}_{\mathrm{m}} = 0 \\ \frac{\mathrm{d}}{\mathrm{d}t} S = 0 &\Leftrightarrow \frac{\mathrm{d}}{\mathrm{d}t} \tilde{\omega}_{\mathrm{m}} = 0 \end{aligned} \qquad [4.106]$$

The dynamic of the system taken out of the observation error takes the following form:

$$-\frac{P_{\mathrm{p}}}{J_{\mathrm{m}}} \cdot T_{\mathrm{l}} - k_1 \cdot \mathrm{sgn}\left(\tilde{\omega}_{\mathrm{m}}\right) = 0 \qquad [4.107]$$

Consequently, the equation verified by the load torque observed on the sliding surface is written as:

$$\frac{\mathrm{d}}{\mathrm{d}t} T_{\mathrm{l}} = \frac{k_2}{k_1} \cdot \frac{1-\lambda}{T_{\mathrm{e}}} \cdot \frac{P_{\mathrm{p}}}{J_{\mathrm{m}}} \cdot T_{\mathrm{l}} \qquad [4.108]$$

Gain k_2 then sets the dynamic of the load torque observation convergence on the S sliding surface.

4.8.4. *Presentation of observer performances*

4.8.4.1. *The shattering phenomenon*

The shattering phenomenon accompanies the non-linear techniques of control or observation. It is characterized by a variation band of the observed value, in the case studied, speed and load torque (Figure 4.41), around its true value. First, we examine it in the case where controlled speed is measured; the VSMO then operates in open loop in relation to control. The simulation result proposed in Figure 4.41 was obtained for the following test protocol [ARC 99]:

1. {0 s–0.4 s}: machine magnetization;
2. {0.4 s–1.4 s}: machine acceleration to rated speed;
3. {1.4 s–2 s}: sinusoidal mode operation;
4. {2 s–2.5 s}: load impact with a value 80% of nominal torque.

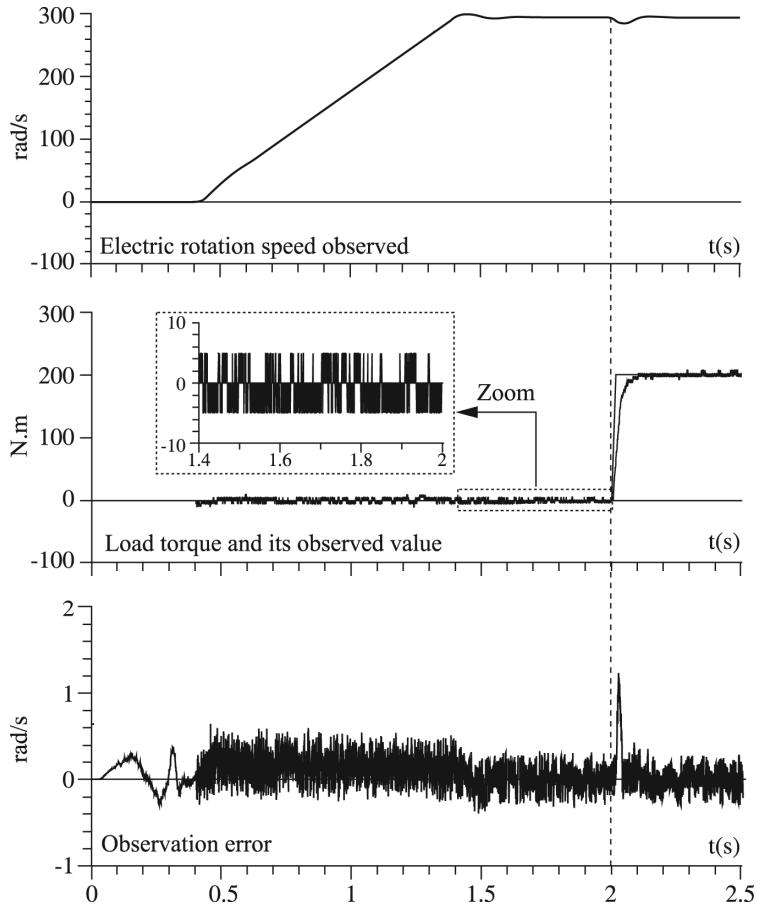

Figure 4.41. *Illustration of the shattering phenomenon*

The commutation term chosen to build this VSMO involves the signum function (Figure 4.42a) of the error between a value that we can measure and its observed value. It makes it possible to maintain the observed value on the *S* sliding surface. This very quick phenomenon is a hindrance when the observer is introduced in the direct torque control.

To reduce this effect, we can add a saturation function (Figure 4.42b) where discontinuities around zero are not as abrupt.

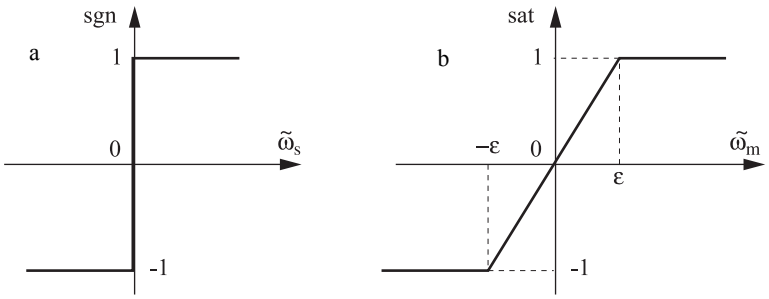

Figure 4.42. *Commutation functions*

We can observe the improvement of the waveform on the observation of mechanical speed (Figure 4.43), and even more clearly on the observation of the load torque.

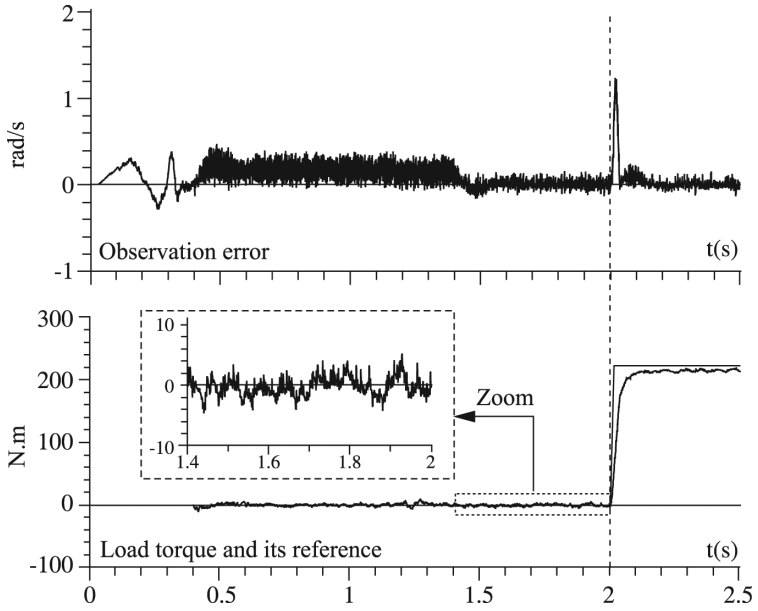

Figure 4.43. *Limitation of the shattering phenomenon with the help of a saturation function*

4.8.4.2. *Rated speed operation*

We will now use the observer based on the structure proposed in Figure 4.40. The variable structure observer is defined by equation [4.100]. In this case, the

commutation function "sgn" is replaced by the saturation function in order to limit the shattering phenomenon. The gains of matrix L are chosen with the help of a pole placement technique.

Figure 4.44 presents the results obtained for the same test protocol as the one applied to the previous two simulations. We notice that observation errors of the mechanical speed and load torque are more significant than those in Figure 4.43.

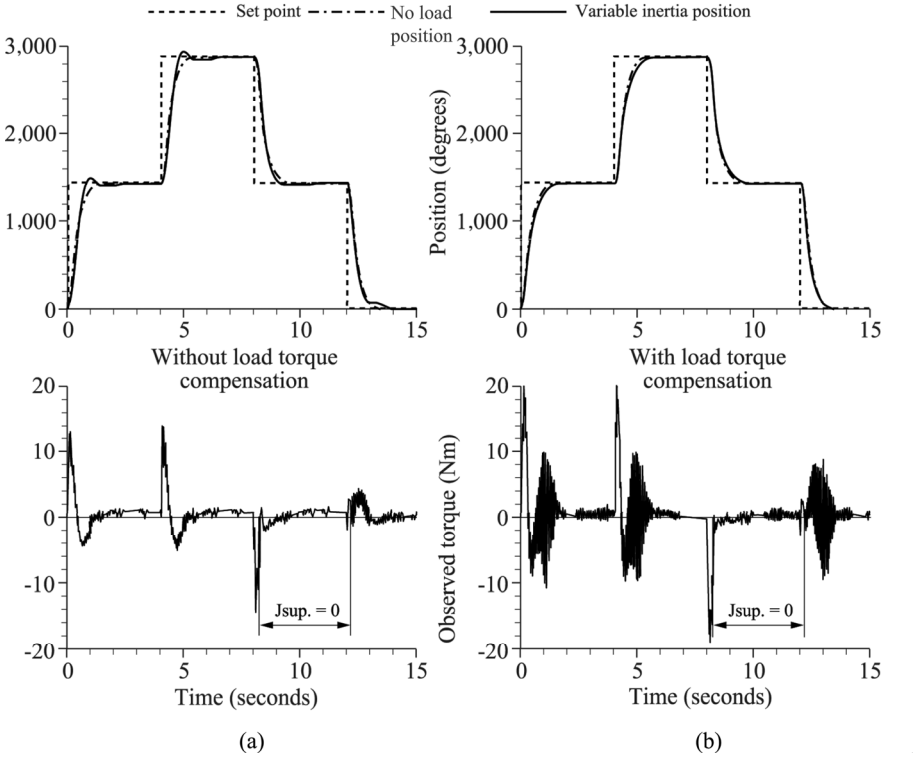

Figure 4.44. *Observation of mechanical speed and load torque by the VSMO*

This test highlights the influence of inaccuracies on the value of the mechanical speed obtained by the selfpiloting relation, which plays a role of "measurable" variable in the VSMO. They can therefore be studied as measuring errors. The sliding surface that was chosen first, according to equation [4.102], is no longer suitable and must be replaced by surface S_1:

$$S_1 = \hat{\omega}_m - \left(\hat{\omega}_s + \hat{\omega}_r + \nu\right) \quad [4.109]$$

where ν represents estimation errors.

If estimation errors are marked [4.102], then S_1 sliding surface becomes a band around the true value to observe, and where the width is based on the upper boundary of inaccuracies [ARC 99].

In the literature, the variable structure observer is reputed for its remarkable robustness in relation to measuring errors notably. In reality, we notice that these measuring errors are reinjected by the term $L \cdot \tilde{\omega}_m$ (linear part) and by the commutation term characteristic of non-linear observers $K \cdot \text{sgn}\left(\tilde{\omega}_m\right)$. This commutation term participating in the VSMO convergence provides greater impassivity to measuring errors. It is disrupted by the other term that only widens the direct attraction area of the sliding surface and weakens observer robustness in relation to measuring errors. The results presented in Figure 4.45 are obtained for an observer structure where the term $L \cdot \tilde{\omega}_m$ is cancelled as above:

$$\frac{d}{dt}\hat{X}_m = A_m \cdot \hat{X}_m + B_m \cdot U_m + K \cdot \text{sgn}\left(\hat{\omega}_m - \omega_m\right) \quad [4.110]$$

with $\hat{X}_m = \begin{pmatrix} \hat{\omega}_m \\ \hat{C}r \end{pmatrix}$ and $K = \begin{bmatrix} -k_1 \\ -k_2 \end{bmatrix}$.

The protocol for the test development is as follows [ARC 99]:

1. {0 s–0.4 s}: installation of the machine flux;

2. {0.4 s–0.6 s}: machine acceleration to rated speed;

3. {0.6 s–1.4 s}: sinusoidal mode operation;

4. {at t = 1 s}: load impact with a 70% of nominal torque value;

5. {1.4 s–1.8 s}: reversal of the load rotation direction of the machine;

6. {1.8 s–3 s}: sinusoidal mode operation;

7. {at t = 2.5 s}: disappearance of the constant load with a 70% of nominal torque value;

8. {3 s–3.2 s}: deceleration to zero speed.

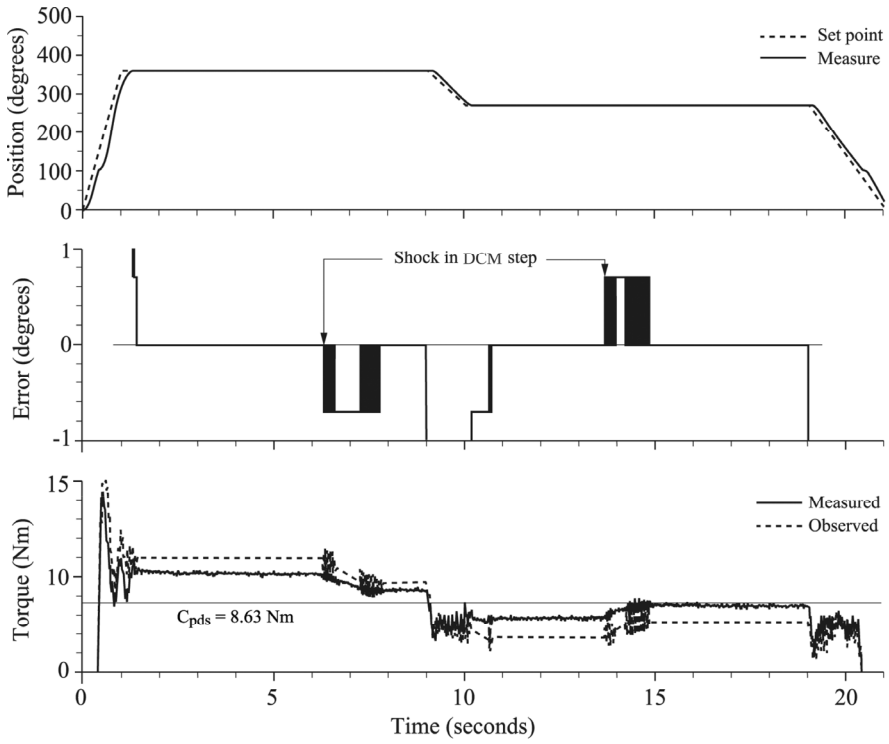

Figure 4.45. *Observation of mechanical speed and load torque with VSMO structure [4.110]*

4.8.5. *Low-speed operation*

We will now study the behavior of the VSMO at low speed. We recall that the introduction of an observer able to provide a mechanical speed value and a load torque value is particularly interesting when we want to compensate the influence of the latter.

The results of the two following figures show the performances obtained for low-speed operation, at 6% of rated speed, with a control that is previously described (Figure 4.46) and where the load torque value is compensated from the variable structure observer with equation [4.110].

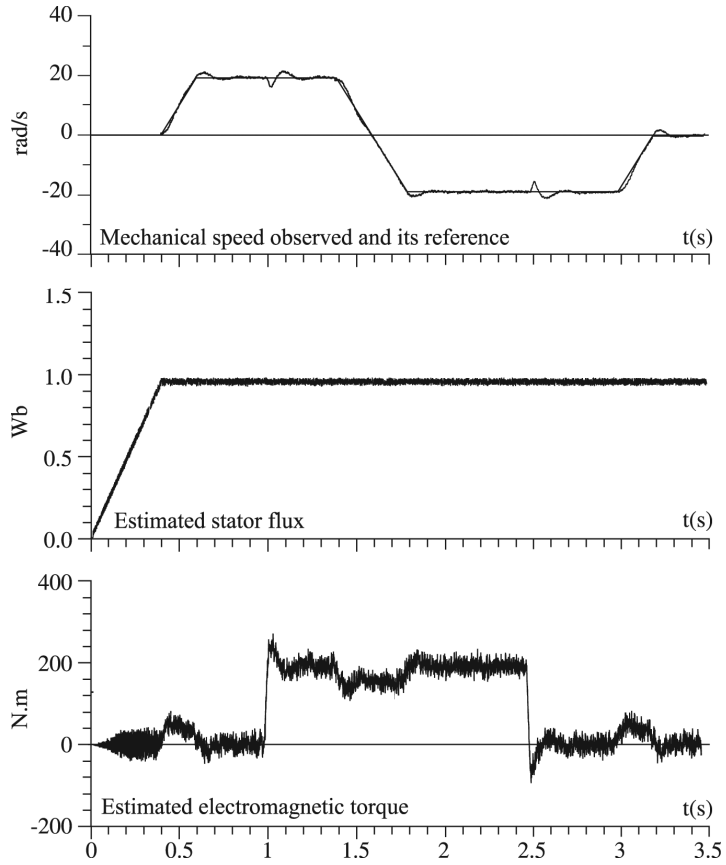

Figure 4.46. *Load torque compensation through the variable structure observer of the mechanical speed and load torque*

The load torque compensation enables the proportional–integral speed equalizer to be adapted to speed control, in accordance with the synthesis made in relation to its reference. In this way, loss of speed at load impact is lower than 2% of rated speed. The electromagnetic torque rise occurs in less than 20 ms. We then observe a torque rise dynamic of over 50 T_{nom}/s.

The results obtained greatly depend on the VSMO value of commutation gain k_2 adjusting the convergence dynamic of the load torque observation value in the sliding surface [4.102]. The gain value k_2 depends on the compromise between convergence speed of the observer and its sensitivity to measuring errors. The idea is then to establish a compromise between observation precision and electromagnetic torque response dynamic.

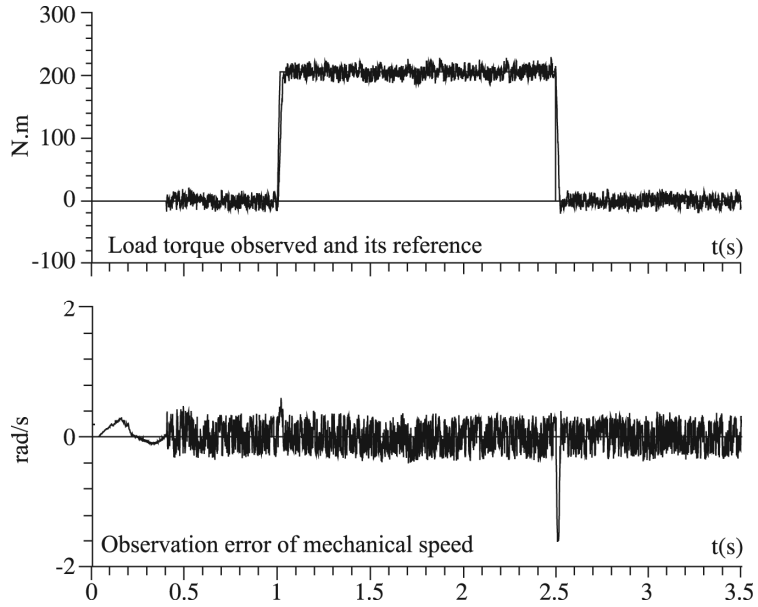

Figure 4.47. *Observation of mechanical speed and load torque at slow operating speed*

4.8.6. *Robustness in relation to parametric variations*

4.8.6.1. *Mechanical parameter variations*

We test the previous VSMO in relation to mechanical parameter variations, that is, viscous friction f_m and moment of inertia J_m. We modify the values of these parameters in the observer model. The case of a 50% underestimation of inertia and the effect of a 75% underestimation of the viscous friction is examined. The case of overestimations lead to conclusions similar to those presented Figure 4.48.

Figure 4.48 illustrates an operation for the following test protocol:

1. {0 s–0.4 s}: machine fluxing;
2. {0.4 s–1.4 s}: machine acceleration to rated speed;
3. {1.4 s–2 s}: sinusoidal mode operation;
4. {2 s–2.5 s}: load impact with a value of nominal torque.

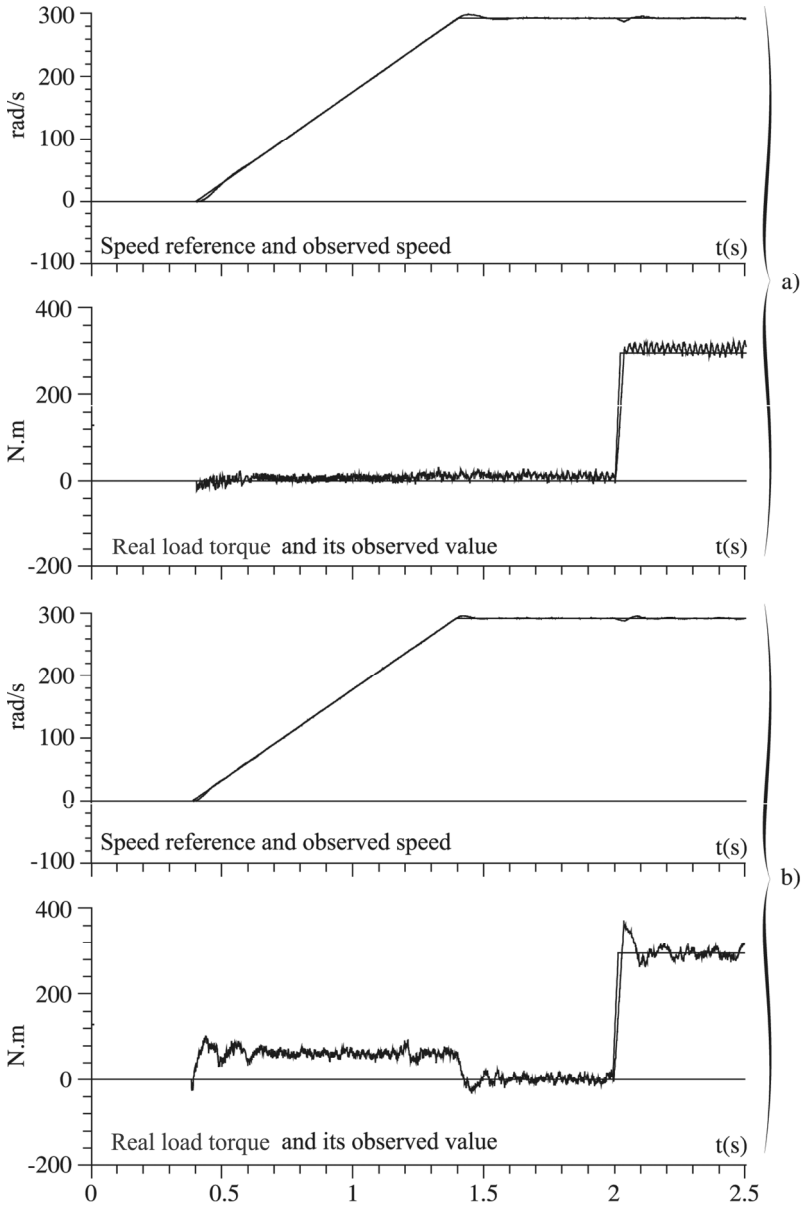

Figure 4.48. *Speed and pump torque response observed at a variation of mechanical parameters: (a)* $f_{\mathrm{m}_{\mathrm{obs}}} = 0.25 \times f_{\mathrm{m}}$, *(b)* $J_{\mathrm{m}_{\mathrm{obs}}} = 0.5 \times J_{\mathrm{m}}$

These first two reports illustrate the influence of an underestimation of the viscous friction factor (a) and the last two illustrate the effect of an underestimation of inertia (b). We can observe that these two errors are processed by the observer as if it were an additional load torque. In case (a), this gap corresponds to a term $\Delta f_m \cdot \omega_m$, and in the second case (b), it corresponds to an additional fictitious inertial load [ARC 99]. However, the gap between observation of load torque and true load torque is completely offset by the regulation maintaining the observed speed at its reference. We thus confirm the global insensitivity of the sensorless control to variations of the installation's mechanical parameters.

4.9. Conclusion

The estimation and observation problem discussed in this chapter is at the heart of a methodology, leading to research in efficient and powerful control of an induction machine desired by the industrial world. Although it is economical to develop and inexpensive to operate, the induction motor drive (of torque, rotation speed, and/or position) requires vector control with a flux that must have imposed orientation. Consequently, any vector control requires excellent knowledge of the flux vector represented by its module and phase. Since this vital variable is not directly accessible, it must be reconstituted as reliably as possible with the help of flux estimators or observers. These mathematical algorithms are simply indirect sensors, characterized by an inherent dynamic and able to define the flux module and its position in a more reliable manner. Although the open loop estimation structures are simple, they lack parametric robustness and their dynamic is greatly linked to that of the system. The different observer structures function in closed loop, their dynamic is independent from that of the system, and their parametric robustness is better than the estimators. Both structures can be defined in the different reference frames, linked to stator, rotor, or rotating field. The search for a model for an observation is therefore a very important step and, as was presented, the stationary–reference frame is the best one adapted for flux observation and estimation. Deterministic observers and estimators suppose that the model is perfectly well known and they ignore the hazards linked to noises from the system and measures. Since precise knowledge of the system is impossible because of the different uncertainties, stochastic observers were developed guaranteeing more reliable, efficient, and powerful overall operation of the variable speed drive. The Kalman filter made it possible to consider the characteristics of noises and system imperfections, while ensuring parametric robustness. These structures were introduced in different vector controls known for their performance and high dynamic. But these different strategies are very often associated with a suppression of the mechanical sensor, leading to a search for sensorless control. In this chapter, "partial" estimation or observation methods were presented; they help reconstitute the rotation speed without questioning the initial structure of the control working with the

sensor. It is important to carefully verify the performances of the induction variable speed drive in every aspect of operation and especially at low speeds. In order to improve the global behavior of the variable speed drive, we must use a global flux observation and speed method.

4.10. Bibliography

[AND 96] ANDREAS PURWOADI M., Réglage non linéaire du variateur de vitesse asynchrone sans capteur de vitesse, Doctoral Thesis, INPT, Toulouse, June 1996.

[ARC 99] ARCKER-HISSEL A.M., Contrôle direct du couple électromagnétique de machines asynchrones de grande puissance, Doctoral Thesis, INPT, Toulouse, February 1999.

[BUH 86] BÜHLER H., *Réglage par mode de glissement*, Presses polytechniques romandes, Switzerland, 1986.

[CAR 95] CARON J.P., HAUTIER J.P., *Modélisation et commande de la machine asynchrone*, Editions Technip, Paris, 1995.

[CHA 83] CHATELAIN J., *Machines électriques*, vol. 1, Editions Dunod, Paris, 1983.

[BEN 93] BEN AMMAR F., Variateur de vitesse de hautes performances pour machine asynchrone de grande puissance, Doctoral Thesis, INPT, Toulouse, April 1993.

[FOR 97] DE FORNEL B., PIETRZAK-DAVID M., ROBOAM X., "State observers for control of A.C., variable speed drives", *EPE-PEMC, 7th International Power Electronics and Motion Control Conference and Exhibition*, vol. 2, p. 1–7, Budapest, Hungary, September 2-4, 1997.

[JAC 95] JACQUOT B., Conception, étude et réalisation des algorithmes de commande des systèmes de traction asynchrone pour les TGV de nouvelle génération, Doctoral Thesis, INPT, Toulouse, December 1995.

[JAN 94] JANSEN P., LORENZ R., "A physically insightful approach to the design and accuracy assessment of flux observers for field oriented induction machine drives", *IEEE Transactions on Industry Applications*, vol. 30 no. 1, p. 101–109, January 1994.

[KAL 82] KALMAN R.E., "A new approach to linear filtering and prediction problems", *Transactions of the ASME. Series D, Journal of Basic Engineering*, p. 35-45, 1982.

[LUE 71] LUENBERGER D.G., "An introduction to observers", *IEEE Transactions on Automatic Control*, AC–16, p. 596-603, December 1971.

[OUR 95] OURTH T., Commande vectorielle d'un moteur asynchrone sans capteur de vitesse. Observateur déterministe de flux rotorique, Doctoral Thesis, INPT, Toulouse, November 1995.

[PIE 88] PIETRZAK-DAVID M., Algorithmes de commande d'un variateur électrique asynchrone: contrôle dynamique du flux, commande optimale en position, Doctoral Thesis, INPT, Toulouse, 1988.

[PIE 00] PIETRZAK-DAVID M., DE FORNEL B., ROBOAM X., "Estimations et observations déterminismes et stochastiques des états électromagnétiques", *Commande des moteurs asynchrones*, vol. 2, Hermes, Paris, 2000.

[POP 73] POPOV V.M., *Hyperstability of Control System*, Springer-Verlag, Berlin, 1973.

[ROB 92] ROBOAM X., HAPIOT J.C., DE FORNEL B., ANDRIEUX C., "Contrôle d'une machine asynchrone par estimation robuste de la vitesse", *Journal de Physique III*, no. 2, p. 439-453, 1992.

[SIA 92] SIALA S., Motorisation asynchrone d'un robot mobile. Observation et régulation du flux, Doctoral Thesis, INPT, Toulouse, February 1992.

[SCH 92] SCHAUDER C., "Adaptive speed identification for vector control of induction motor without rotational transconductors", *IEEE Transactions on Industrial Applications*, vol. 28 no. 5, 1992.

[UTK 81] UTKIN V.I., *Sliding Modes in Control Optimization*, Springer-Verlag, Berlin, 1981.

[WES 94] VON WESTERHOLT E., Commande non linéaire d'une machine asynchrone, Doctoral Thesis, INPT, Toulouse, March 1994.

[VUL 98] VULTURESCU B., BOUSCAYROL A., IONESCU F., "Model influence on simulation of induction machine vector control", *Advanced Topics in Electrical Engineering Conference, ATEE-98*, Bucharest, p. 137-142, 1998.